Published in final edited form as:
*J Phys Chem B*. 2008 September 18; 112(37): 11679–11693. doi:10.1021/jp8038835.

# Electrostatic Properties of Aqueous Salt Solution Interfaces: A Comparison of Polarizable and Non-Polarizable Ion Models

**G. Lee Warren** and **Sandeep Patel***
Department of Chemistry and Biochemistry, University of Delaware, Newark, Delaware 19716, USA

## Abstract

The effects of ion force field polarizability on the interfacial electrostatic properties of ~1 M aqueous solutions of NaCl, CsCl and NaI are investigated using molecular dynamics simulations employing both non-polarizable and Drude-polarizable ion sets. Differences in computed depth-dependent orientational distributions, “permanent” and induced dipole and quadrupole moment profiles, and interfacial potentials are obtained for both ion sets to further elucidate how ion polarizability affects interfacial electrostatic properties among the various salts relative to pure water. We observe that the orientations and induced dipoles of water molecules are more strongly perturbed in the presence of polarizable ions via a stronger ionic double layer effect arising from greater charge separation. Both anions and cations exhibit enhanced induced dipole moments and strong *z* alignment in the vicinity of the Gibbs dividing surface (GDS) with the magnitude of the anion induced dipoles being nearly an order of magnitude larger than those of the cations and directed into the vapor phase. Depth-dependent profiles for the trace and *zz* components of the water molecular quadrupole moment tensors reveal 40% larger quadrupole moments in the bulk phase relative to the vapor mimicking a similar observed 40% increase in the average water dipole moment. Across the GDS, the water molecular quadrupole moments increase non-monotonically (in contrast to the water dipoles) and exhibit a locally reduced contribution just below the surface due to both orientational and polarization effects. Computed interfacial potentials for the non-polarizable salts yield values 20 to 60 mV more positive than pure water and increase by an additional 30 to 100 mV when ion polarizability is included. A rigorous decomposition of the total interfacial potential into ion monopole, water and ion dipole, and water quadrupole components reveals that a very strong, positive ion monopole contribution is offset by negative contributions from all other potential sources. Water quadrupole components modulated by the water density contribute significantly to the observed interfacial potential increments and almost entirely explain observed differences in the interfacial potentials for the two chloride salts. By lumping all remaining non-quadrupole interfacial potential contributions into a single “effective” dipole potential, we observe that the ratio of quadrupole to “effective” dipole contributions range from 2:1 in CsCl to 1:1.5 in NaI suggesting that both contributions are comparably important in determining the interfacial potential increments. We also find that oscillations in the quadrupole potential in the double layer region are opposite in sign and partially cancel those of the “effective” dipole potential.

*Corresponding author. sapatel@udel.edu.

**Keywords**

AIR/WATER INTERFACE; SURFACE; SALTS; SIMULATIONS; MOLECULAR DYNAMICS; ELECTROLYTE SOLUTIONS; SODIUM CHLORIDE; SODIUM IODIDE; CESIUM CHLORIDE; SURFACE POTENTIAL; INTERFACIAL POTENTIAL; QUADRUPOLE MOMENT

## I. INTRODUCTION

With the heightened sensitivity to global environmental and climatological trends of the past decade, much attention has been focused towards understanding heterogeneous chemical processes occuring in higher regions of the atmosphere. One area of intense current research activity concerns atmospheric reactions generating molecular halogen species with concomitant ozone uptake into mobile aqueous sea-salt based aerosols and droplets.[1–3] Field experiments in conjunction with aerosol chamber kinetics measurements and computational modeling[4] have suggested the presence of halide anions in the interfacial regions of the aqueous salt droplets. X-ray photoelectron spectra[5] also indicate a surface enhancement of anions at aqueous solution interfaces. Moreover, advances in non-linear vibrational spectroscopies such as SFG[6–11] and SHG[12–15] in conjunction with molecular dynamics simulations of aqueous salt solutions[16–23] have provided a new paradigmatic view of these interfaces which is characterized by the density enhancement of large, polarizble anions in the outermost interfacial layer (in the vicinity of the Gibb's dividing surface). The prevailing physical justification for this observed surface density enhancement is that strong anion-water induced dipole interactions accompanying asymmetric surface solvation easily offset the energetic penalty associated with partial anion desolvation at the surface. While the polarizability of the anionic species and the solvent are significant contributors to this phenomenon, several additional factors have also been implicated including the size of the ions, entropic effects arising from solvent structure and reorganization, ion surface charge density, the magnitude of the water dipole moment (and its variation in the asymmetric interfacial region), and the particular nature of the solvation shell surrounding the ion.[18,19,23–31] Overall, large, softer anions such as $Br^-$ and $I^-$ exhibit prominent surface effects, whereas small, hard anions such as $F^-$ show negligible surface density enhancement.

As suggested in the preceding paragraph, modeling and theoretical approaches have significantly contributed to a microscopic understanding of the interfacial structure and thermodynamics of aqueous salt solutions and have helped to facilitate the interpretation of experimental findings. In particular, polarizable molecular models which incorporate dipole induction effects appear to be an indispensable tool for obtaining an accurate theoretical estimation of solution structure and thermodynamics in such interfacial systems. The development of novel non-additive, or polarizable, force fields for inorganic ions,[32–37] small molecules,[33,38–41] and larger biologically relevant macromolecules42–51 has attracted considerable interest and has resulted in the development of several conventional approaches for modeling atomic and molecular polarization. These approaches include point-dipole (and higher-order multipole) polarizable models,[39,41,52–54] Drude oscillator models,[36,40,55–58] and charge equilbration/fluctuating charge models[42–45,59,60,60–67] in addition to fully *ab*

*initio* based approaches such as Car-Parrinello molecular dynamics techniques.[68–70] A significant body of work has explored the behavior of point-dipole polarizable models of pure water, aqueous ionic solutions, and other small, strongly-associating molecules at liquid-vapor interfaces.[13,16,18–23,32,69,71–74] Unfortunately, similar studies quantifying the effects of ion and water polarization on interfacial structure and thermodynamics using alternative approaches are rather rare in the literature. In particular, the behavior of charge equilibration models with respect to modeling the liquid-vapor interfaces of aqueous electrolyte solutions has not been characterized in detail, though studies have explored various other dynamical and thermodynamic properties of charge equilibration water models.[51,75] These models represent an efficient alternative to standard point-dipole polarizable models and, of particular significance, permit a representation of multipole electrostatic induction contributions beyond simply the dipole polarizability response. Such interactions may play an important secondary role in determining the structure and dynamics of solvated ions near the surface of aqueous solutions where strong electrostatic induction effects play a key role.

While a variety of recent studies[20,68,71] have discussed electrostatic properties of aqueous solutions of monovalent ions including dipole moment orientational profiles of water and ions across the liquid-vapor interface, very few studies have provided a detailed investigation of the interfacial electrostatic potential. Specifically, the effects of explicit inclusion of ion model polarization on the predicted electrostatic interfacial potential has not been addressed. The electrostatic potential provides complementary information on orientational order at the interface. Furthermore, since most studies implement point-dipole polarizable electrostatic models, decomposition of the interfacial potential into contributions from dipole and higher order moments, i.e. the quadrupole moment in the case of water, has not been systematically addressed. These contributions, nevertheless, are critical to understanding the underlying driving forces for ion surface enhancement and layering effects. In addition, the molecular physics directing water orientation in the interfacial region is intimately associated with a microscopic understanding of ionic solvation. Numerous studies[19,21,71,72,76–79] have considered the relationship between electrostatic effects at aqueous and aqueous electrolyte surfaces and water orientational structure, dipole orientational profiles and the interfacial potential. For neat water solutions, the total interfacial potential is commonly decomposed into a dipole orientational contribution[76,80] and a water quadrupole moment contribution.[81,82] Unfortunately, recent investigations of aqueous electrolyte solutions[20,71,72] commonly partition the total interfacial potential into a static (fixed charge) contribution and an induced dipole contribution both of which are quite large in magnitude and opposite in sign and lead to significant cancellation which masks more subtle features of the underlying molecular physics.

This contribution extends our previous work wherein we explored specific effects of ion polarizability on interfacial properties and characterized differences in structural properties arising from the inclusion of ion polarizability. In the present study, we attempt to quantify differences in electrostatic properties of aqueous interfacial systems containing simple monovalent ions and illuminate the role of interfacial dipole and quadrupole potentials in these systems. In the following sections, we discuss the models employed in our

simulations, orientational, dipole moment, and quadrupole moment profiles for water and the polarizable ion models as a function of depth and specific features of and contributions to the interfacial electrostatic potentials in these systems.

## II. THEORY AND METHODS

### A. Force fields

In this study, we investigate the effects of ion force field polarizability on the interfacial electrostatic properties of several aqueous monovalent salt solutions. Such two-phase systems consisting of a solution in equilibrium with its vapor require the use of polarizable water models since fixed-charged models parameterized according to the average electrostatic environment of the isotropic bulk phase cannot optimally model the low density vapor side of the interface. Previous work has highlighted significant differences between non-polarizable and polarizable water models with respect to water translational diffusion[75,83–85] and hydrogen bonding populations[69,78] and dynamics[75,86] in the vicinity of the liquid-vapor interface. In the interfacial region, the dipole moments of the individual solvent molecules monotonically transition from a large condensed phase value to a much weaker gas-phase value.[20,52,68,78,87,88] To model this effect, we have chosen to employ the polarizable TIP4P-FQ (Transferable Intermolecular Potential Four Point Fluctuating Charge) water model of Rick *et al*.[59] to describe the water component of the solution-vapor interfaces. The TIP4P-FQ model is a rigid water model, characterized by a single Lennard-Jones interaction site placed on the oxygen atom and a massless, off-atom *M*-site which carries the instantaneous oxygen partial charge. The TIP4P-FQ model yields average gas and condensed phase dipole moments of 1.85 D and 2.62 D, respectively, which are in reasonable agreement with both experiment[89,90] (1.86 D and 2.96 ± 0.6 D) and *ab initio* molecular dynamics simulations[69,78,88] (2.9 to 3.0 D in the condensed phase) as well as other common water force fields which yield condensed-phase total dipole moments in the range of 2.18 to 3.02 D.[69] In addition, the TIP4P-FQ model also allows for quadrupole moment induction through the redistribution of molecular partial charge which is not permitted in many other commonly used rigid dipole polarizable water models. Consequently, contributions to interfacial properties arising from quadrupole moment induction remain largely uncliaracterized in aqueous interfacial systems.

To model the ions, we have considered two sets of ion models; the first set consists of non-polarizable models[91] in which electrostatic interactions are described by fixed, unit point charges while the second set consists of a set of dipole-polarizble Drude models.[92] Both ion model sets are derived from the AH/SWM4-DP ion models of Lamoureux and Roux[36] which were developed in conjunction with the simple water model with four sites and Drude polarizability[55] and parameterized to reproduce gas phase cluster enthalpies and bulk hydration free energies. The present ion models all share the same Lennard-Jones parameters and differ only in the inclusion of Drude polarizability. For the present Drude models, the ion polarizabilities have been slightly reduced[92] with respect to their original values[36] to account for differences in polarizability anisotropy between the presently employed TIP4P-FQ water model and the SMW4-DP water model to which the Drude ion models were originally parameterized. Complete details regarding the construction,

implementation and performance of the current ion models are described in our previous work.[91,92]

### B. Simulation methodology

Molecular dynamics simulations are performed using Chemistry at HARvard Molecular Mechanics (CHARMM) package[93] version 34a1 with custom modifications to permit the simultaneous propagation of fluctuating and Drude charges. SHAKE[94] constraints are utilized to enforce a rigid water geometry. All Lennard-Jones interactions are smoothly tapered to zero at distance of 12 Å over a 1 Å range. Long-range electrostatic interactions are handled using the smooth particle mesh Ewald[95,96] (PME) method.

Approximately 1 M aqueous solutions of NaCl, CsCl and NaI are assembled from 988 TIP4P-FQ water molecules and 18 cation-anion pairs. Interfacial systems are prepared by the three dimensional periodic replication of a rectangular unit cell having dimensions of 24 × 24 × 100 Å that is approximately half-occupied by solution. This yields a periodic slab geometry in which each cell contains two explicit vapor-solution interfaces separated by approximately 48 Å of solution. All interfacial systems are sampled under conditions of constant temperature and volume (*NVT*) for a total of 80 ns following 500 ps of initial equilibration from a previously equilibrated geometry. More specific details regarding our employed simulation protocols may be found in reference 92.

## III. RESULTS AND DISCUSSION

### A. Density profiles

The computed density profiles for neat water and for the six salt solutions which we investigate here have been examined in detail in an earlier study.[92] Therefore we will provide only a brief overview of some pertinent aspects of these density profiles and direct the reader to figure 8 of reference 92 and the associated discussion for further details. A sample profile for the Drude-polarizable NaI solution is plotted in figure 1. The *z* axis describes the distance in angstroms from the Gibbs dividing surface (GDS) (marked by a vertical line) which delineates the point at which the surface excess of the water component is zero. The profiles for all three solution components (water, cations and anions) are normalized relative to the densities obtained from simulations of the corresponding periodic bulk systems.[92] Thus, it is clear from figure 1 that the density of sodium and iodide ions in the bulk region of the slab is only 93% of the estimated bulk value. The depletion or enhancement of ion density in the bulk region is important as it shows whether there is a net excess or depletion of ion density at the surface which, depending on the magnitude and sign of the surface excess, is related to changes in surface tension via the Gibbs isotherm equation. For the six salt solutions investigated, only the Drude-polarizable NaI solution demonstrates a net depletion of ions in the bulk region; all others show a weak to moderate increase in ion density in the bulk which, on average, is greater for the non-polarizable ions. Thus, ion polarizability appears to slightly reduce the bulk excess in favor of a surface excess.[92]

For the polarizable salt models, we observe significant local density enhancement of the anions at the interface which is consistent with the results of a number of recent

theoretical[12,16,18–23,79] and experimental[4,5] investigations. In contrast, the non-polarizable salts show only weak anion attraction to the interface. For the density profiles which show moderate to substantial surface enhancement of the anions (such as in figure 1 for polarizable NaI), the large surface density is followed by a considerable sub-surface density depletion of anions and an local excess of cation density. Far away from the interface, both ion densities plateau to the same value as required by the condition of electro-neutrality. These oscillatory density distributions lead to an overall separation of anion and cation density at the interface (an ionic double layer effect) that creates a strong electric field. This electric field has substantial perturbative effects on the distribution of solution components and the orientation of solvent molecules in the interfacial region.

### B. Orientational distributions

To analyze the orientational structure of the water molecules in both neat water and the various salt solutions, we use two coordinates, $\theta$ and $\varphi$ to characterize average orientation as a function of depth[17,20,76] (figure 2). The coordinate $\theta$ represents the polar angle that the "permanent" molecular dipole vector (taken to be the magnitude of the dipole moment in the gas phase) makes with the fixed $\hat{z}$ axis of the unit cell (i.e. the vector normal to the water surface). Zero angles are indicative of strongly aligned orientations in which both water hydrogens point toward the vapor phase. Similarly, angles near 90° represent orientations in which the molecular symmetry axis lies parallel with the interfacial plane. In this work, we have chosen to report averaged distributions for the cosines of these angles rather than for the bare angles themselves which permits convenient comparison with prior work. Additionally, the distribution of the $z$ projection of the water permanent molecular dipole moments may be trivially obtained from the angular distribution $\langle \cos\theta \rangle$ by scaling it by the gas phase TIP4P-FQ dipole moment of 1.85 D.

Complete orientational disorder of the water molecules leads to an average value of zero for the distribution $\langle \cos\theta \rangle$ in the bulk liquid; however, zero values of $\langle \cos\theta \rangle$ may also arise from cancellation between equal populations of aligned and anti-aligned molecules. To distinguish between these possibilities, we make use of a second angular coordinate, $\varphi$, which describes the dihedral angle that the water molecular plane makes with the $\hat{z}$ axis of the unit cell (panel B of figure 2). Values of $\varphi$ near 90° ($\cos\varphi = 0$) correspond to configurations in which the water molecular plane lies parallel to the Gibbs dividing surface (CDS); likewise, for values of $\varphi$ near 0° or 180° ($\cos\varphi = 1$ and $-1$), the molecular plane is oriented perpendicular to the interfacial surface. Since both water hydrogens are equivalent by symmetry and $\varphi = 180$ and $\varphi = 0$ both lead to indistinguishable perpendicular orientations, we find it convenient to employ the distribution $\langle |\cos\varphi| \rangle(z)$ in which values close to 1 and 0 describe the perpendicular and parallel orientations, respectively. Thus, in the bulk region where the angular distribution is isotropically disordered, we obtain an expected value for this function of 0.5 (60°) due to the two-fold multiplicity of the perpendicular orientations.

In figure 3 we have plotted $\langle \cos\theta \rangle$ as a function of the distance $z$ from the CDS for neat TIP4P-FQ water and 1 M solutions of NaCl, CsCl and NaI. Results for the non-polarizable salts are presented in panel A and those for the Drude polarizable salts in panel B. The

corresponding distributions of $\langle|\cos\varphi|\rangle(z)$ are plotted in panels A and B of figure 4. In the bulk liquid near the slab centers and far from the liquid-vapor interface, both distributions approach a constant value consistent with complete orientational disorder due to the isotropic bulk environment. At approximately 4 Å to 6 Å beneath the CDS and coincident with regions of enhanced cation density (see figure 1 and figure 8 of reference 92), we note maxima in the $\langle\cos\theta\rangle(z)$ distributions for all salt solutions (both polarizable and non-polarizable) accompanied by only slight differences in the distribution $\langle|\cos\varphi|\rangle(z)$ over the same region. This effect is stronger for the more surface active ion models and indicates a preference for the water molecules to orient their dipole moment vectors toward the vapor phase. As previously noted,*20* net water orientation in the interfacial region is largely modulated by the separation of the ions in the *z* direction into layers parallel to the GDS in which the average position of the anions is nearer to the vapor phase than that of the cations. This charge separation generates a weak, local electric field which reorients nearby waters. From an examination of the corresponding z-dependent density profiles,*92* we see that interfacial depths ranging from $z = -5$ to $z = -6$ (where the reorientation effect is strongest) describe crossover regions in which the cation density begins to exceed the anion density with increasing depth. Thus, water molecules in this cross-over region between the oppositely charged double layers experience the strongest electric fields and preferentially reorient to place hydrogens nearer to the interface in the direction of the excess local anion density. Consequently, the height of the corresponding peak in $\langle\cos\theta\rangle(z)$ in the same region correlates with the strength of the charge layering effect and is strongest for the polarizable models which yield a larger average charge separation. In our salt solutions containing non-polarizable ions, the primary charge layering effect extends to a considerable depth within the interface. In contrast, no maximum is observed in the corresponding distribution for neat TIP4P-FQ water (for which there is no ionic double layer effect). The absence of a prominent second peak in the orientational profiles of all three polarizable and non-polarizable salt solutions confirms that secondary ion layering effects are unimportant at these ion concentrations.

In the region $-5.0$ Å$< z < 0$ Å, just beneath the GDS, $\langle\cos\theta\rangle(z)$ for all three salt solutions and for neat water decreases sharply to a minimum. For neat water and the two non-polarizable chloride salts, the average orientation of water in this region tends slightly toward the bulk solution*82* (evidenced by $\langle\cos\theta\rangle(z) < 0$). Compared with the results for the flexible-polarizable (FP) water model of Ishiyama and Morita,[20] the neat TIP4P-FQ liquid exhibits 2 to 3 times smaller values of $\langle\cos\theta\rangle$ in this region. As seen in the plot of $\langle|\cos\varphi|\rangle(z)$ in figure 4, this is complemented by TIP4P-FQ's strong preference for orientations parallel to the interface. Thus, relative to the FP water model, there appears to be an increased propensity for the TIP4P-FQ molecules in this region to lie flat or parallel to the interfacial plane but slightly tipped so that both hydrogens point toward the bulk. This behavior is somewhat surprising considering the model's lack of out-of-plane polarizability and may be a consequence of quadrupole effects (both permanent and induced). In the case of the salts, we also observe minima similar to that of pure water in the same region. However, for all solutions except those of the non-polarizable chloride salts, the net water orientation is reversed (positive values of $\langle\cos\theta\rangle(z)$) so that the water hydrogens remain preferentially oriented toward the vapor phase over the entire 15 Å interfacial region. This

change in orientation accompanies the increased anion density at and above the GDS which implies that the water hydrogens are simply reorienting in the presence of a strong charge layering effect to point toward the excess anion density. We also note that in the plot of $\langle|\cos\theta\rangle(z)$, the minima near $z = -2$ assume less positive values. Since the position of the minima correlate with regions of maximal anion density, we surmise that this is a consequence of enhanced lateral anion-water interactions which encourage water dipole moments to orient parallel with the interfacial plane. While this effect is strongest for the polarizable ion models and presumably enhanced by the anion induced dipole moments in the case of the polarizable models, it is still present (though to a lesser degree) in the case of the non-polarizable ion models; therefore, it is not exclusively an effect of ion polarizability.

On the vapor side of the GDS, we observe that water molecules adopt perpendicular orientations relative to the interfacial plane so that one water hydrogen is on average directed away from the liquid, consistent with prior observations of dangling or free OH bonds at the surface.[17,20,76,82] This picture is complemented by a prominent maximum in the $\langle|\cos\varphi|\rangle(z)$ distribution just above the GDS indicating significant $z$-alignment of the water molecules in this region. We also note that the structure and placement of this peak is consistent for all salts and for neat water suggesting that water orientational features of the vapor side of the interface are not strongly perturbed by the presence of the anions (though they are somewhat shifted in the case of the polarizable ion models). Similar findings regarding the relatively weak perturbation of water above the GDS have been reported*20* in simulations employing *polarizable* ions for which the surface concentration of anions is weakly to moderately enhanced. In the vapor phase beyond a distance of 4.0 Å from the GDS, the statistical sampling becomes increasingly poor due to the small number of molecules present in the vapor phase.

### C. Water dipole moment distributions

A number of previous investigations of aqueous interfaces have found that water models incorporating polarization effects can lead to structural and dynamical interfacial properties qualitatively distinct from those of fully non-polarizable models. For instance, Liu, Harder and Berne[75] report faster hydrogen bonding dynamics at the interface relative to the bulk for polarizable water models (and in particular for the TIP4P-FQ model) which is opposite to the behavior observed[84] for fixed-charge models. This is thought to arise from stronger water-water pairing and increased translational diffusion in the lower density regions at and above the GDS. Since an analysis of the permanent and induced water dipole moments relative to the gas phase structure is also an obvious metric for judging the impact of polarization on the interfacial properties (both of neat water and the corresponding salt solutions), we compute $z$-dependent distributions for the average induced dipole moment and the average $z$-projection of the induced dipole moment of interfacial water molecules.

In general, the average total water dipole moment monotonically decreases from the average bulk value of 2.62 D deep within the water slab to a value of 1.85 D in the vapor phase. The profile for the average water induced dipole moment (not shown) has a shape similar to that of the total dipole moment and for the present model monotonically decreases from a bulk value of 0.83 D to a value of zero in the vapor phase. We note that the bulk value of 0.83 D

is slightly larger than the value of 0.77 D obtained from the simple difference one might obtain between the magnitude of the averaged total condensed phase dipole moment of 2.62 D and the magnitude of the gas phase dipole moment of 1.85 D. This difference arises from the instantaneous correlation between the permanent and induced dipole vectors which is included in the latter estimate but not in the former. We remark that the average water induced dipole moment profile is consistent in both shape and magnitude to profiles reported for other water models.[20,69,78,79]

Since differences in the water induced dipole moment profiles among all of the salt solutions are small and difficult to distinguish between the profiles, we have chosen instead to plot in figure 5 the average magnitude of the water induced dipole moments $\langle \mu \rangle$ less that of pure TIP4P-FQ water $\langle \mu \rangle_w$ as a function of depth $z$ to better exhibit the differences. Results for the non-polarizable and polarizable salt models are plotted in panels A and B, respectively, of figure 5. Overall, we note only small perturbations (< 0.05 D) in the total water induced dipoles due to the presence of the ions. Curves for the non-polarizable and polarizable ion models are quite similar and maintain the same relative shifts. However, one small but noticeable difference between the non-polarizable and polarizable ion profiles is the appearance of a single broad peak approximately 3 Å beneath the CDS in the case of the polarizable models signifying an overall (weak) enhancement of the water induced dipole moments. These peaks are only present for the polarizable ion models (all of them) and appear to achieve maximum intensity in center of the double layer region. Since these peaks are not present for any of the non-polarizable salts, we conclude that this is not simply a double layer effect arising from an enhanced water response to the perturbed electric field since the non-polarizable salts should also show some effect (in particular for non-polarizable Nal). Instead, this feature appears exclusively attributable to ion polarizability and the presence of ion induced dipoles in this region which cooperatively reinforce the induced dipoles of the surrounding water molecules.

The average $z$-projection of the water induced dipole moment vectors as a function of $z$ are plotted in figure 6 for the non-polarizable ion models (panel A) and the Drude polarizable ion models (panel B). In the bulk, far from the interface, the largely isotropic environment yields an expected $z$-induced dipole moment of zero in each case. As we approach the GDS from the bulk side, we observe that $\langle \mu_{I,z} \rangle$ rises to a maximum in the salt solutions as we transition through the electric double layer. In this region the water induced dipoles are oriented slightly toward the vapor phase and point in the same direction as the water permanent dipole moments (as indicated by the maximum in the distribution $\langle \cos \theta \rangle(z)$ in figure 3). The effect of the ionic double layer on the water induced dipoles is stronger for the polarizable salt models (by approximately a factor of 2 to 3) owing to the greater charge separation in these systems. This feature is, of course, absent for neat water for which there is no double layer effect.

In the region $-5 < z < 3$, we observe a rapid transition in the induced dipole orientation for neat water and for all salt solutions as we cross the GDS from the bulk into the vapor phase. All of the $z$-induced dipole profiles are negative in this region indicating a net orientation of the induced dipoles toward the bulk phase. At and above the GDS, we observe in all cases that the induced dipole moments point slightly toward the bulk phase in opposition to the

contributions of the permanent dipole moments which, from the respective orientation distributions (figure 3), point slightly into the vapor. For the salt solutions, this net orientation of surface induced dipoles opposes that of the induced dipoles in the sub-surface region.

Interestingly, we observe for the TIP4P-FQ model that the *z* components of the induced water dipole moments are three to four times larger than those previously reported for the FP model[20] and indicate a significant water model dependence in the observed interfacial structure which, in the present case, is undoubtedly influenced by the unique polarizability anisotropy of the TIP4P-FQ water model. The strongest induced dipoles in the region $0 < z < 3$ are observed for neat water and are on the order of −0.2 D. For the non-polarizable ions, we observe little or no perturbation of the profiles at and above the GDS demonstrating that the overall electrostatic structure of the water remains relatively undisturbed by the introduction of the ions. However, for the more surface active polarizable ion models, we see a reduction in the net orientation of the induced dipoles and a shift toward larger values of *z* coinciding with the appearance of increased anion density at and above the GDS. This trend may be indicative of a larger percentage of surface waters reorienting their induced dipoles laterally so that they point toward the anions instead of toward the bulk.

### D. Water quadrupole moment distributions

Having thoroughly characterized the water permanent and induced dipole moment distributions, we extend our analysis to include averaged distributions of the water quadrupole moments. Such distributions are important in the present case because our chosen solvent model, TIP4P-FQ, models polarizability by the redistribution of molecular charge which can result in the induction of higher-order electrostatic moments in addition to the usual induced dipole moment. In contrast, other commonly used rigid Drude and single point dipole models do not make allowance for quadrupole induction; notable exeptions include the AMOEBA water model[53] which permits point-dipole induction on each atomic site as well as various flexible models in which the quadrupole moment can change via structural perturbations. Thus, it is important to examine the behavior of the induced quadrupole response and consider the impact of this model aspect on various interfacial properties.

In figure 7 we plot the average magnitude of the *zz* component of the molecular quadrupole moment as a function of depth for both the non-polarizable (panel A) and polarizable (panel B) salt models. The *zz* components are taken from the traced form of the molecular quadrupole tensor $\Theta$ expanded about an origin placed on the oxygen site. All salt models appear to result in similar orientationally averaged gas and condensed phase moments of 0.13 $e$Å$^2$ and 0.185 $e$Å$^2$, respectively. Thus, we see an increase of 0.055 $e$Å$^2$ (~40%) in the average *zz* component of the quadrupole moment as we cross into the liquid from the vapor which is comparable to the concomitant ~40% increase in the average water dipole moment. We note that this change is non-monotonic and demonstrates a strong oscillation in the vicinity of the GDS for all salt solutions. Since it is also present for neat water, this oscillation does not arise from an ionic double layer effect but is instead related to the orientation and polarization of the water molecules at the interface. Since the out-of-plane

direction will yield the smallest *zz* projection of the quadrupole moment, it is likely that the minimum values observed near the GDS derive from the propensity for water molecules to lie more parallel with the interfacial plane as described in figure 4 for the angular distribution function $\langle |\cos \varphi| \rangle (z)$. Similarly, the region just above the GDS in which free OH bonds extend into the vapor phase would be expected to yield a larger *zz* quadrupole moment contribution which is indeed consistent with figure 7. In keeping with the picture of fully solvated anions at the surface of the non-polarizable salt solutions, we see relatively small perturbations of the corresponding quadrupole moment profiles. However, for the polarizable salt models, we observe stronger perturbations in the double layer region between $z = -5$ Å and $z = 1$. Interestingly, the *zz* projection of the water quadrupole moments increase in magnitude in the region occupied by the cation excess and decrease in the region near the GDS occupied by the polarizable anions.

We also note that between the polarizable and non-polarizable salts, the relative ordering of the bulk phase average moments are preserved. A corresponding plot of the average trace of the quadrupole moment tensor, $\langle \mathrm{tr}(\boldsymbol{\Theta}) \rangle (z)$, (not shown) demonstrates similar structural features and rises from a value of 0.38 $e$Å$^2$ in the vapor to a value of 0.55 $e$Å$^2$ in the bulk region, consistent with values computed from the average gas and bulk phase partial charges. One small difference between the trace and *zz*-component profiles is that the depth of the minimum near the GDS is reduced due to inclusion of the transverse components of the quadrupole moment tensor. However, this feature does not disappear completely and, since we have averaged out the orientational dependence by taking the trace, the remaining contributions to the depth of the minimum must arise from polarization effects. This polarization effect is rationalized by considering the *z* component of the water induced dipole moments (figure 6) which in the vicinity of the GDS are oriented somewhat opposite to the permanent dipole moments components which follow the angular distribution $\langle \cos \theta \rangle (z)$ in figure 3. Induced dipole moments which oppose the fixed molecular dipole moments imply that the molecular charge redistribution is working to decrease the magnitudes of the hydrogen and oxygen partial charges; this appears consistent with the smaller observed quadrupole moment trace and *zz* projection and demonstrates a unique effect of employing a quadrupole-polarizable model that will impact other computed interfacial properties such as the surface potential.

### E. Ion dipole moment distributions

Complementary to the induced dipole moment profiles for water, we also examine induced dipole moment profiles for the anions and cations in the simulations employing polarizable ion models. For the anions in each salt solution, we have plotted the total magnitude of the anion induced dipole moments in panel A of figure 8; the corresponding *z* components appear in panel B. For the present anion models, we observe a steady, monotonic increase in both the total and *z* components of the anion dipole moments across the GDS beginning at $z = -5$ A and peaking near $z = +2.5$ Å. Over the same region, the *z* components of the induced dipole moments (2.5 D for NaI and 1.9 D for NaCl and CsCl) comprise a large percentage (80 to 90%) of the total induced anion dipole moments. At 5 Å from the GDS, the total induced dipoles have fully relaxed to their respective vapor (0.0 D) and bulk (1.75 D for NaI and 1.25 D for NaCl and CsCl) values. The magnitude of our observed bulk and maximum

interfacial anion induced dipole moments appear consistent with the work of Wick and Dang[71] who report values of approximately 2.2 D (bulk) and 3.4 D (interface) for $I^-$ in 1 M Csl solutions at the aqueous vapor interface. Ishiyama and Morita[20] (which for their flexible-polarizable water model observe more modest surface anion enhancement) report similarly shaped but less intense profiles for the *z* projections of the induced anion dipole moments which reach a maximum of 1.4 D also near $z = +2.0$ Å. For simulations of polarizable NaI in SWM4-DP water[55] using the Drude-polarizable AH/SWM4-DP ion models[36] (the ones on which the present models are based), Archontis *et al*.[79] report a peak value of $+3.92 \pm 0.5$ D for $I^-$ and an average value of $3.40 \pm 0.6$ D in the bulk. These results are somewhat larger than what we obtain for the present models but consistent with the fact that we have artificially reduced the anion polarizabilities for use with TIP4P-FQ water.

In both panels A and B, we note that the $Cl^-$ profiles for the NaCl and CsCl solutions are very similar and show virtually no dependence on the identity of the cation; both chloride salts also appear to yield nearly the same total induced dipole moment in the bulk far from the interface. Interestingly, the profiles of both $I^-$ and $Cl^-$ which differ somewhat in magnitude have surprisingly similar shapes given the numerous differences between the $I^-$ and $Cl^-$force field parameters. While the changes in magnitude may be easily correlated with the increased polarizability of $I^-$, similarities in the shapes of the profiles reflect a consistent water mediated response to the presence of the anions at the surface. Mechanistically, it is thought[19,23,73,77,79] that the enhancement of the anion induced dipoles accompanying desolvation at the interface is stabilized by the local asymmetric electrostatic environment. Below the surface, anions interact strongly with nearby water hydrogens and water molecules tilt their induced dipoles toward the anion; these collective interactions create a strong polarizing electrostatic environment which (owing to rapid density falloff of water above the GDS) is negligibly counter-balanced by water interactions on the vapor side. The strong uni-directional polarizing environment beneath the anion coupled with the large polarizability of the anions results in strong anion polarization at the interface in which the anion induced dipole moments point into the vapor phase.

We have also computed profiles of the total and *z* components of the cation induced dipole moments in panels A and B, respectively, of figure 9 for the Drude polarizable ion models. As expected, we find nearly negligible total induced dipole moments for $Na^+$. The total induced moment for $Cs^+$ in the bulk liquid is approximately five times larger than that of $Na^+$ but still an order of magnitude smaller than the bulk induced dipole moment of the corresponding $Cl^-$ counter-ion. Overall, the largest contributions from the cation induced dipole moments are obtained from the few cations sampled in the vicinity of the GDS. These contributions are of opposite sign compared with those of the anions and disagree with the findings of reference 79 which report a positive (vapor oriented) *z* dipole moment on the order of +0.03 D for $Na^+$ in polarizable NaI solutions (though the reported error bar is on the order of half a Debye). The present behavior is not surprising if one considers that a cation on the surface largely sees a bulk solution with an excess negative charge and vice versa for the anions. Thus the cation will orient its induced dipole to point toward solution while the anions will direct theirs away. Also, since the cations overwhelmingly remain fully coordinated (even near the surface), we also expect the sign of the induced cation dipole

moment to mimic the directionality of the induced dipole moments of the surrounding waters which (from panel B of figure 5 also point toward the liquid phase. A close comparison of the anion and cation profiles for the *z* components of the induced dipoles also reveals that the maximum in the cation induced dipole distribution lies 1 to 2 Å closer to the GDS than that of the anion distribution. Thus, the largest induced cation moments arise from cations just beneath the outermost layer of anions. However, we note that statistically, there are very few configurations in which the cations visit this region as evidenced by the larger amount of noise in the profiles near and above the GDS.

### F. Solution-vapor interfacial potential

A sensitive measure of the combined electrostatic effects of the water orientation, ion distribution, and induced dipole moment distributions of the various components at the interface is the potential drop associated with bringing a positive test charge from the vapor phase into solution. This difference in electrostatic potential, termed the interfacial potential, results from a net orientation of dipole moments (both permanent and induced for all solution components) in addition to a quadrupole moment contribution (permanent and induced) arising from the distribution, orientation and density of water molecular quadrupole moments. While this property is conveniently accessible in simulation, consensus experimental estimates of the interfacial potential (even for pure water) remain in dispute and include both positive and negative values that span an approximate ±1500 mV range around zero (see references 97 and 98 and the references contained therein). In contrast, a number of recent theoretical determinations of the inter facial potential of water derived from molecular dynamics simulations employing a variety of water models and simulation protocols typically report consistent values on the order of -400 to -600 mV (discussed below). This consistency is reinforced by the common use of an unambiguous protocol for evaluating the surface potential which involves a straightforward integration of the charge density. Wilson *et al*.[99] have demonstrated that the total interfacial potential obtained in this way may be further decomposed into dipole and quadrupole contributions. It has been argued[100] that experimental determinations of the interfacial potential which employ probes of atomic dimensions having an excluded volume cannot sample the electrostatic potential within the interior of molecules; consequently the resulting potential values are not directly comparable to those determined via test charges having no excluded volume, e.g. potentials derived from direct integration of the charge density. Thus, the dipole component of the interfacial potential arising from net water orientation at the interface (often termed the *surface* potential) is sometimes considered[99] to be a more suitable quantity for comparison with experiment. Consequently, in the present work we separate these contributions to the interfacial potential in order to stimulate further discussion and facilitate future comparisons with experiment. To avoid confusion, we will use the term “interfacial potential” in the remainder of this work, unless otherwise indicated, when referring to estimates of the total potential drop which include quadrupole contributions (such as those obtained by integration of the charge density). Similarly, we will refer to the dipole component of the interfacial potential as the “surface potential.”

We compute the solution-vapor interfacial potential, $\Delta\Phi$, for a planar interface by integration of the *z* component of the charge density,[55,60,77,82,99,101,102] $\rho(z)$, according to

$$\Delta\Phi(z) = \Phi(z) - \Phi(z_0) = -\frac{1}{\epsilon_0}\int_{z_0}^{z} dz' \int_{z_0}^{z'} dz'' \rho(z'') \quad (1)$$

where the coordinate $z$ is along the direction of the surface normal and $z_0$ corresponds to the center of the water slab. Numerical integration is performed by the evaluation of the charge density over discrete slabs of 0.1 Å thickness along the $z$ direction. The computed interfacial potentials for TIP4P-FQ water and 1 M salt solutions of NaCl, CsCl and NaI are plotted in figure 10 for the non-polarizable (panel A) and polarizable (panel B) salt models. We note that with the present degree of sampling, interfacial potentials for all systems are well converged to within approximately 5 mV (table I) in the central regions of the slabs. For neat TIP4P-FQ, we obtain a converged interfacial potential of −529 ± 2 mV which is in excellent agreement with our previously reported[91] value of −527 mV for this model and consistent in magnitude with a variety of estimates obtained for other polarizable[20,55,77] and non-polarizable[77,82] water models.

Within approximately 6 Å of the GDS, we note some small oscillations (< 15 mV) in the interfacial potential of pure water along with the conspicuous absence of a prominent (20 to 80 mV) minimum at $z = -2$ Å which has been observed for some polarizable water models such as SWM4-DP,[55] the Dang-Chang model[52,69,72,77] and the flexible-polarizable model of Ishiyama and Morita[20] as well as some non-polarizable models including SPC/E[82] and TIP4P.[77,103,104] In previous work[91] employing a smaller system containing 432 waters and significantly less sampling, we observed a small (~40 mV) well for the TIP4P-FQ model; thus, the improved sampling in the present case yields a smaller well depth relative to the bulk potential though there is little difference between the present and prior estimates of the bulk value of the potential. Interestingly, the location of the potential well correlates with that of a small previously noted[92] plateau in the water density located approximately 2 to 4 Å below the GDS which is also more fully sampled in the present work. Since for water the total interfacial potential is determined by the partial cancellation between a positive dipole contribution related to the orientation of surface waters and a negative quadrupole contribution arising from the water quadrupole moment density, we surmise that the reduced density in the plateau region yields a locally diminished quadrupole moment contribution to the total interfacial potential which, in turn, reduces the well depth. However, we also note that while the absence of a prominent well in the present case may reflect a peculiarity of the TIP4P-FQ model (perhaps arising from the unique polarizability anisotropy of this model or the inclusion of an induced quadrupolar response), it may also be sensitively affected by the choice of simulation, Ewald and histogramming protocols which vary considerably among the cited estimates.

For the non-polarizable salt models, we obtain converged, bulk potential values of −511 ± 4 mV, −467 ± 4 mV and −508 ± 5 mV for NaCl, CsCl and Nal, respectively, which correspond to increments in the interfacial potential (**ΔΔΦ**) of 18, 62 and 21 mV relative to that of neat TIP4P-FQ water (table I). For the polarizable salt models NaCl-D, CsCl-D and Nal-D, we obtain values of −481 ± 4 mV, −440 ± 5 mV and −410 ± 8 mV, respectively, which correspond to **ΔΔΦ** values of 48, 89 and 119 mV. All computed interfacial potentials appear to be fully converged to their corresponding equilibrium values at depths of 15 to 18

Å beneath the GDS. For some salts such as NaCl, where the degree of charge separation is small, the convergence of the interfacial potential is quite rapid with increasing depth; similarly, the convergence of the potentials with depth for the polarizable salts generally appear slower than for the non-polarizable counterparts. Both observations indicate that perturbations arising from strong charge layering effects penetrate to significant depths into solution.

Approximately 2 to 3 Å below the GDS, we observe pronounced minima in the total interfacial potentials for both the polarizable and non-polarizable salts. The depth of these minima relative to the asymptotic bulk potential values appear to correlate with the strength of the double layer effect and are deepest for the surface active, polarizable salts. Also for the polarizable salts, we notice some minor shifting of the minima closer to the GDS which is strongest for Nal-D and is consistent with the *z* positioning of the respective anion densities which for $I^-$ lies closest to the vapor phase[92] (as judged relative to the position of the GDS).

Overall, for both the polarizable and non-polarizable salt models, we observe total interfacial potentials more positive than that of neat water in agreement with the findings of various recent studies[20,71,72] and reviews.[19,21] However, the reported magnitudes of the observed potential shifts relative to that of neat water vary considerably and appear to have a significant water and ion model dependence.[21,103,105] For example, using polarizable water and ion models, Wick, Dang and Jungwirth72 have computed shifts of 30 to 40 mV in ~1 M KC1 salt solutions which are quite comparable to our observed shifts for the polarizable models of the chloride salts. In contrast, Ishiyama and Morita[20] report considerably smaller shifts of 1 mV and 31 mV for ~1.1 M solutions of NaCl and Nal, respectively, which are more comparable to our observed shifts for the non-polarizable salt models. A much larger shift of 150 mV has been obtained by Wick and Dang[71] for ~1 M Csl solutions which, considering separately our observed shifts for CsCl and Nal, appears consistent with our current estimates for the Drude-polarizable salt models. Furthermore, our estimates of the interfacial potential shifts agree reasonably in magnitude with the commonly cited[18,19,71,72] experimental measurements of Randies[106] for various aqueous electrolyte solutions.

A visual comparison of panels A and B of figure 10 reveals that the magnitude of the potential shifts relative to neat TIP4P-FQ water are larger for the polarizable salt models. Interestingly, the relative ordering of NaCl and CsCl is maintained between the non-polarizable and polarizable salt models with CsCl > NaCl by approximately 40 mV regardless of whether ion polarizability is present; however, when Drude polarizability is introduced into the NaI model, the response is dramatically different with $\mathbf{\Delta\Delta\Phi}$ changing from a value of 21 mV (close to that of non-polarizable NaCl) to a value of 119 mV (significantly above that of polarizable CsCl). To assess the impact of ion polarizability on the interfacial potential increments, we compute the quantity $\mathbf{\Delta\Delta\Phi}_{\mathrm{poi}}$ given by the difference between the $\mathbf{\Delta\Delta\Phi}$ values of the polarizable and non-polarizable models. We obtain values of $\mathbf{\Delta\Delta\Phi}_{\mathrm{poi}}$ of 30, 27, and 98 mV for NaCl, CsCl and Nal, respectively. Apparently, the interfacial potentials of both chloride salts are affected similarly by the presence of ion polarizability; likewise a larger perturbation is observed for NaI; this is not surprising given that the iodide anion has a polarizability greater than twice that of chloride. These findings

also appear to show that changes in the interfacial potential arising from ion polarizability are negligibly affected by the identity of the cation.

Considering how similarly ion polarizability affects both NaCl and CsCl, it is natural to inquire as to why the interfacial potential shifts for these salts (table I and panels A and B of figure 10) are so different, being separated by approximately 40 mV. To tackle this question, we consider a decomposition of the total potential according to the monopole, dipole and quadrupole contributions. More specifically, the more positive interfacial potential values of the salt solutions arise from several potential sources: monopole contributions due to the different z-dependent physical distributions of the ionic point charges ($\mathbf{\Delta\Phi}_q(M^+A^-)$), water permanent and induced dipole contributions ($\mathbf{\Delta\Phi}_M(H_20)$), ion induced dipole contributions ($\mathbf{\Delta\Phi}_M(M^+A^-)$), and water quadrupole contributions ($\mathbf{\Delta\Phi}_Q(H_20)$). A breakdown of the total interfacial potentials into these components is provided in table I for each salt solution investigated.

Several important observations are made in the case of the water quadrupole moment contributions to the interfacial potential which are computed from the local molecular quadrupole density $Q_{zz}(z)$ as

$$\Delta\Phi_Q(z) = -\frac{1}{\epsilon_0}\left[Q_{zz}(z) - Q^{\circ}_{zz}\right] \quad (2)$$

relative to a reference value $Q^{\circ}_{zz}$ taken to be zero and situated far away in the vapor phase. The local molecular quadrupole moment density is then defined[99,107] as

$$Q_{zz}(z) = \left\langle \sum_m \delta(z - z_m)\left(\frac{1}{2}\sum_i q_{im} z_{im}^2\right)\right\rangle \quad (3)$$

where the indices *m* and *i* denote a molecule and an atomic site within that molecule, respectively. In expanding the molecular moments, we take the oxygen atom to be our molecule-specific center, $z_m$. The resulting quadrupole components of the interfacial potentials (which from table I appear to be similar in magnitude) are plotted in figure 11, panel A, for the various polarizable salt solutions less the contributions from neat TIP4P-FQ water. Surprisingly, differences in the bulk quadrupole potentials appear to qualitatively account for a large portion of the observed potential increments, particularly for the chloride salts (both non-polarizable and polarizable); likewise the difference in $\mathbf{\Delta\Delta\Phi}$ for the two chloride salts (approximately 40 mV) can be almost fully explained by the differences in the respective quadrupole moment contributions (approximately 35 mV). This indicates that changes in the quadrupole contributions within the bulk liquid significantly contribute to the overall observed bulk potential increments.

In isotropic phases, it is common to estimate the total bulk quadrupole moment contribution $\mathbf{\Delta\Phi}_Q$ via the simple formula[99,100,108,109]

$$\Delta\Phi_Q \approx -\frac{\rho\gamma}{6\epsilon_0} \quad (4)$$

where $\rho$ is the bulk density of solvent molecules and

$$\gamma=\sum_i q_i r_i^2. \quad (5)$$

is the trace or isotropic quadrupole moment of a single solvent molecule which for TIP4P-FQ water is approximately equal to 1.11 $e$Å$^2$. In a non-isotropic environment such as our aqueous interfacial systems, the density will carry a $z$ dependence and the $zz$ components of the molecular quadrupole moments will change based on the local average molecular orientation and partial charges. By noting the water density dependence of equation 4 and by making use of the $z$ dependent water density profiles for the salt solutions ($\rho(z)$) and neat water ($\rho_w(z)$), we may construct a new quadrupole potential $\Delta\Phi'_Q$ as

$$\Delta\Phi'_Q(z)=\frac{\rho_w(z)}{\rho(z)}\Delta\Phi_Q(z) \quad (6)$$

which effectively rescales the contributions according to changes in the local water density relative to the pure water density at the same distance from the GDS. This function is plotted for the polarizable salts as a function of $z$ in panel B of figure 11. The modified quadrupole potentials yield bulk values that differ by less than ±10 mV from that of neat TIP4P-FQ water. Therefore, we conclude that the quadrupole moment contributions arising from differences in the water density in the interfacial systems almost entirely account for the differences in the observed bulk quadrupole contributions. Thus it is quite possible for the non-polarizable salt models which demonstrate reasonable bulk water densities in interfacial salt solutions to yield qualitatively correct interfacial potential shifts. Panel B of figure 11 also demonstrates that the remaining quadrupole contributions near the GDS which arise from orientational and polarization effects in the double layer region negligibly influence the bulk potentials due to nearly complete cancellation of the positive and negative oscillations; thus, ion polarizability primarily affects the bulk quadrupole moment contributions through the physical redistribution of ion density accompanying surface enrichment (which in turn impacts the water density distribution). Consequently, we also expect that induced water quadrupole moments arising from molecular charge redistribution in the double layer region to only weakly affect the bulk interfacial potential (though they may have larger effects on other computed interfacial properties).

In a similar manner, it is also advantageous to consider the remaining (non-quadrupole) components of the interfacial potential. Several prior studies[20,71,72] have investigated the induced (ion + water) dipole contributions separately from the permanent (ion + water) multipole components. For solutions of Csl and KC1, Wick and coworkers[71,72] have found both contributions to be large in magnitude, relatively featureless and opposite in sign so that the total potential is derived from significant cancellation of the two contributions. Ishiyama and Morita[20] report a similar cancellation between the permanent and induced components for ~1.1 M solutions of NaCl and NaI. From this cancellation, it is clear that there is a large degree of interdependency between the permanent multipole and induced dipole components that masks some of the more subtle features of the interfacial potential components. Therefore in the present decomposition, we find it advantageous to examine

the sum of all the remaining components (essentially the total interfacial potential less the quadrupole contribution which we have just examined separately above). Our motivation is two-fold. First, for the salt solutions, this yields contributions comparable to the total dipole potential of neat water (which is the only remaining component for the pure water system). Thus, the combined action of the ion monopole distribution, the induced ion and water dipole distributions and the water permanent dipole distribution creates an "effective" dipole or surface potential drop. Second, we feel that this "effective" dipole potential, analogous to the water dipole potential in pure water (which also excludes the quadrupole contributions) is a more suitable quantity for comparison with some experimental determinations of the *surface* potential.

To assemble these "effective" dipole potentials, we compute separately the ion monopole contributions, the total (permanent plus induced) water dipole contributions and the ion induced dipole contributions. The monopole contributions are obtained from equation 1 by only integrating over the ionic charge density of the ions. The water and ion dipole potentials are obtained by integration over the *z*-component of the respective dipole moment densities $P_z(z)$ of water and the ions according to the formula*99,107*

$$\Delta\Phi_{\mathrm{M}} = -\frac{1}{\varepsilon_0}\int_{z_0}^{\infty} dz \quad P_z(z). \quad (7)$$

The dipole moment density $P_z(z)$ is defined as

$$P_z(z) = \left\langle \sum_m \delta(z - z_m) \left( \sum_i q_{im} z_{im} \right) \right\rangle \quad (8)$$

in a manner analogous to the quadrupole moment density above (equation 3). For the bulk, values of the individual components are listed in table I. We note that the present decomposition fully accounts for all contributions since in all cases the total interfacial potential obtained by integration of the charge density is equal to the sum of the decomposed components to within the reported errorbars. The resulting "effective" dipole potential functions assembled from these components are plotted in figure 12 less the dipole potential profile of neat water. First, we note that the shifts associated with the "effective" dipole potentials of NaCl-D and CsCl-D are very similar (around 25 mV) and differ only by about 5 mV in the bulk. In contrast, the "effective" dipole potential of Nal-D contributes a shift of almost 75 mV to the bulk value of the interfacial potential. Comparing these potentials with the quadrupole contributions in figure 11, we see that the quadrupole and "effective" dipole contributions in NaCl are almost equal (approximately 25 mV each) and that both contribute positively to raise the total surface potential. In CsCl, the quadrupole contribution is almost twice that of the "effective" dipole contribution, confirming that the difference in the observed surface potential increments for NaCl-D and CsCl-D are almost completely due to the bulk quadrupole contribution. In Nal, the "effective" dipole contributions are 50% larger than the quadrupole contributions (75 mV vs 50 mV) again demonstrating that both components contribute significantly to the total observed potential shift. In the double layer region of the salt solutions, we observe strong oscillations of the "effective" dipole potential shifts that are opposite in sign to those of the quadrupole component (panel A of figure 11)

which are roughly 50% weaker. Thus, we find that the quadrupole moment contributions in the double layer region partially cancel those of the “effective” dipole potential.

Several other interesting observations may be made from the decomposition of the interfacial potential presented in table I. First, we see that overall, the quadrupole components among all the salt solutions are consistent in both sign and magnitude. However, the water total dipole components change dramatically from a value of +594 mV in neat water to a value of -4047 mV in the Drude-polarizable NaI solutions. For all of the salts except non-polarizable CsCl, the sign of the water total dipole component is reversed from the contribution in neat water and increases substantially in magnitude with increased anion surface enhancement due to water reorientation and water dipole induction in the ionic double layer region. The water response works to oppose the positive interfacial potential contribution arising from the charge-layered ion monopoles which are equally large in magnitude. The ion induced dipole contributions are more moderate in magnitude and appear to mimic the behavior of the water dipole contributions in both sign and relative magnitudes between the salts.

Recent work has indicated that polarizable anions are driven to surface by the presence of a free energy minimum in this region[19,21,77,110] arising from the asymmetric solvation environment and the ability of the anion to form a large induced dipole to compensate for the energetic penalty of partial desolvation. Since the cations are repelled from the surface, this leads to the observed charge separation and ionic double layer structure commonly observed in inorganic salt solutions. Our decomposition of the interfacial potential reveals that this charge separation creates an extremely large potential difference which is alleviated (to a large degree) by the water permanent and induced dipole contributions. Water quadrupole contributions supply the remaining deficiency primarily through a redistribution of water density which is slightly increased in the double layer region. The addition of anion polarizability allows the anions to partially recover water dipole contributions lost to the decrease in average molecular dipole density accompanying the presence of non-polarizable ions. This is inferred from ion dipole potential contributions which largely mirror the water dipole potential contributions.

## IV. CONCLUSIONS

In this study we have carried out lengthy molecular dynamics simulations of three different ~1 M aqueous salts solutions to determine the effects of ion model polarizability on the electrostatic properties of the vapor/solution interfaces. By comparing and contrasting results derived from two different ion sets, one in which the ions are modeled as non-polarizable point charges and the other in which ion polarizability is described by classical Drude oscillators, we elucidate the ways in which ion polarizability alters molecular orientations, water fixed and induced dipole and quadrupole moments, ion induced dipole moments, and ion monopole contributions to the interfacial potential as a function of depth.

Overall, we note significant changes in the orientations of water accompanying the introduction of ion polarizability that primarily arise from water reorientation in the presence of the electric field generated by enhanced charge separation. Water molecules

respond by more strongly orienting their molecular dipole moments toward the vapor phase to counter-balance the strong electric field created by the enriched surface concentration of anions which is directed toward the bulk. This has the consequence of reversing the orientation of water in the 5 Å sub-surface region in going from pure water to a finite ion concentration. Above the GDS, the qualitative features of the orientational distributions for all salt solutions are relatively consistent and display dangling or free OH bonds which point into the gas phase. We note some minor shifting of features in this region due the positioning of the anion densities in the *z* direction which for the polarizable ion models lie closer to the vapor phase. Thus, shifting in this region may simply reflect the different intrinsic sizes of the various anions present in the topmost molecular layers.

An investigation of the water induced dipole moment profiles reveals a small enhancement of the induced dipole magnitudes in the double layer relative to pure water. This effect is only observed for the polarizable ion models and appears to be a cooperative effect between the water and ion induced dipoles which is greatly enhanced by the presence of a strong double layer field and large anion polarizabilities. A corresponding analysis of the *z*-components of the water induced dipole moments demonstrate significant reorientation with a reversal of direction in the double layer region with the induced dipoles pointing toward the bulk region at and above the Gibbs dividing surface. Stronger effects are observed for the polarizable salt models which display larger sub-surface charge separation. We also find a reduction in the net *z* alignment at the Gibbs dividing surface for the polarizable salt models indicative of stronger lateral interactions with the increased anion density in this region.

A corresponding analysis of the ion induced dipole moments shows strongly enhanced *z* components near the Gibbs dividing surface that account for a large (80 to 90%) portion of the total ion induced dipoles in this region. Dipole moments for the anions, enhanced by the asymmetric solvation environment at the interface, are 40 to 50% larger at the interface than in the bulk. We observe that cation induced dipoles are generally an order of magnitude smaller than those of the anions and directed toward the bulk rather than toward the vapor phase.

Since the present water force field models polarization via the redistribution of molecular partial charges, we have also characterized quadrupole induction effects which influence the total interfacial potential as well as other interfacial properties. Consequently, we investigate changes in the water quadrupole moments as a function of depth and find an approximate 40% increase in the trace and *zz* components of the molecular quadrupole moment tensor as molecules transition from the vapor into solution. This profile is non-monotonic and exhibits a local minimum in the average *zz* component just beneath the Gibbs dividing surface which appears to coincide with net preference of water molecules to adopt orientations in which the water molecular planes lie parallel with the Gibbs dividing surface. While molecular orientation is largely responsible for this local minimum, we observe that quadrupole induction also contributes.

Lastly, we obtain well-converged interfacial potentials for neat TIP4P-FQ water and for the polarizable and non-polarizable salt solutions of NaCl, CsCl and NaI. Consistent with recent

studies we observe a small increase (20 to 120 mV) in the computed interfacial potentials for all of the salt solutions relative to pure water. Values for the polarizable salt models are 30 to 100 mV more positive than those of the corresponding non-polarizable ion models and appear to consistently depend on the identity of the anion, largely irrespective of the identity of the cation. Despite a number of similarities in the ion density profiles and overall structure of the NaCl and CsCl salts, we observe that the interfacial potential shift of CsCl is larger by approximately 40 mV for both the non-polarizable and polarizable salts. The origin of this difference is elucidated by the decomposition of the total interfacial potential into separate quadrupole and "effective" dipole contributions that differs from the commonly employed decomposition of the interfacial potential into permanent multipole and induced dipole contributions. From our analysis, we find that water quadrupole moment contributions are responsible for a significant portion of the total observed potential shifts are often competitive in magnitude with the "effective" dipole contributions; for the Drude-polarizable ion models, both contributions are nearly equal in the case of NaCl, the quadrupole contributions are larger in CsCl by a factor of 2 and for Nal, the "effective" dipole contributions dominate by a factor of 1.5.

Within the charge-separated double layer region of the salt solutions, we observe that the "effective" dipole and quadrupole contributions have opposite sign and yield significant cancellation. We also note that a large portion of the bulk quadrupole moment contributions arise from perturbations to the water density rather than from water orientation or induced quadrupole contributions in the double layer region which yield negligible bulk contributions for all of the salt models due to cancellation from positive and negative oscillations of near-equal magnitude. Since the non-polarizable salts are also capable of perturbing the water density when forming weak double layers, these quadrupole potential contributions help explain why the non-polarizable salt models are also capable of predicting reasonable shifts in the bulk interfacial potential values. Our decomposition of the total interfacial potential into salt monopole, water permanent and induced dipole, water quadrupole and ion induced dipole contributions reveals that negative water and ion contributions counterbalance the strong positive contribution arising from ionic charge separation in the double layer region. This contrasts with the sign of the dipole potential in pure water which is positive. Overall, we find that the quadrupole contributions from all salt solutions are similar in magnitude. Finally, we comment that our computed "effective" dipole potentials (which are analogous to the dipole potential in pure water) yield a fuller understanding of the nature of the electrostatic contributions present at these vapor/solution interfaces and may provide a more convenient basis for comparison with experimental measurements of surface potentials which may not be as sensitive to the quadrupole contributions.

## Acknowledgments

The authors gratefully acknowledge support from the National Institute of Health sponsored COBRE (Center of Biomedical Research) Grant Numbers P20-RR017716 at the University of Delaware (Department of Chemistry and Biochemistry) and P20-RR015588 (Department of Chemical Engineering).

## References


1. Foster KL, Plastridge RA, Bottenheim JW, Shepson PB, Finlayson-Pitts BJ, Spicer CW. Science. 2001; 291:471. [PubMed: 11161198]
2. Seinfeld JH. Science. 2000; 288:285.
3. Hunt SW, Roeselova M, Wang W, Wingen LM, Knipping EM, Tobias DJ, Dabdub D, Finlayson-Pitts BJ. J. Phys. Chem. A. 2004; 108:11559.
4. Knipping EM, Lakin MJ, Foster KL, Junwirth P, Tobias DJ, Gerber RB, Dabdub D, Finlayson-Pitts BJ. Science. 2000; 288:301. [PubMed: 10764637]
5. Ghosal S, Heniniinger JC, Bluhni H, Mun BS, Hebenstreit ELD, Ketteler G, Ogletree DF, Requejo FG, Salmeron M. Science. 2005; 307:563. [PubMed: 15681380]
6. Richmond GL. Chem. Rev. 2002; 102:2693–2724. [PubMed: 12175265]
7. Walker DS, Richmond GL. J. Phys. Chem. C. 2007; 111:8321–8330.
8. Walker DS, Richmond GL. J. Am. Chem. Soc. 2007; 129:9446–9451. [PubMed: 17616192]
9. Schrodle S, Richmond GL. Applied Spectroscopy. 2002; 62:389. [PubMed: 18416896]
10. Chen Z, Ward R, Tian Y, Baldelli S, Opdahl A, Shen YR, Somorjai GA. J. Am. Chem. Soc. 2000; 122:10615–10620.
11. Liu W-T, Zhang L, Shen YR. J. Chem. Phys. 2006; 125:144711. [PubMed: 17042635]
12. Petersen PB, Saykally RJ. Chem. Phys. Lett. 2004; 397:51.
13. Petersen PB, Saykally RJ, Mucha M, Jungwirth P. J. Phys. Chem. B. 2005; 109:10915. [PubMed: 16852329]
14. Petersen PB, Saykally RJ. Ann. Rev. of Phys. Chem. 2006; 57:333. [PubMed: 16599814]
15. Petersen PB, Saykally RJ. J. Phys. Chem. B. 2006; 110:14060. [PubMed: 16854101]
16. Brown EC, Mucha M, Jungwirth P, Tobias DJ. J. Phys. Chem. B. 2005; 109:7934. [PubMed: 16851926]
17. Morita A, Hynes JT. Chem. Phys. 2000; 258:371.
18. Jungwirth P, Tobias DJ. J. Phys. Chem. B. 2001; 105:10468.
19. Jungwirth P, Tobias DJ. Chem. Rev. 2006; 106:1259. [PubMed: 16608180]
20. Ishiyama T, Morita A. J. Phys. Chem. C. 2007; 111:721.
21. Chang T, Dang LX. Chem. Rev. 2006; 106:1305. [PubMed: 16608182]
22. Mucha M, Prigato T, Levering LM, Allen HC, Tobias DJ, Dang LX, Jungwirth P. J. Phys. Chem. B. 2005; 109:7617. [PubMed: 16851882]
23. Vrbka L, Mucha M, Minofar B, Jungwirth P, Brown EC, Tobias DJ. Gurr. Opin. Colloid Interface Set. 2004; 9:67.
24. Herce DH, Perera L, Darden TA, Sagui C. J. Chem. Phys. 2004; 122:024513. [PubMed: 15638604]
25. Stuart SJ, Berne BJ. J. Phys. Chem. 1996; 100:11934.
26. Perera L, Berkowitz ML. J. Chem. Phys. 1993; 99:4236–1237.
27. Eggimann BL, Siepmann JI. J. Phys. Chem. C. 2007 ASAP Article 10.1021, December 12, 2007.
28. Hagberg D, Brdarski S, Karlstrom G. J. Phys. Chem. B. 2005; 109:4111. [PubMed: 16851470]
29. Bhatt D, Newman J, Radke CJ. J. Phys. Chem. B. 2004; 108:9077.
30. Bhatt D, Chee R, Newman J, Radke C. Curr. Opin. Colloid Interface Sci. 2004; 9:145.
31. Stuart SJ, Berne BJ. J. Phys. Chem. A. 1999; 103:10300.
32. Dang LX, Rice JE, Caldwell J, Kollnian PA. J. Am. Chem. Soc. 1991; 113:2481–2486.
33. Smith DE, Dang LX. J. Chem. Phys. 1994; 100:3757.
34. Perera L, Berkowitz MLZ. Phys. D. 1993; 26:166–168.
35. Perera L, Berkowitz ML. J. Chem. Phys. 1992; 96:8288.
36. Lamoureux G, Roux B. J. Phys. Chem. B. 2005; 110:3308. [PubMed: 16494345]
37. Grossfield A, Ren P, Ponder JW. J. Am. Chem. Soc. 2003; 125:15671. [PubMed: 14664617]
38. Dang LX. J. Chem. Phys. 1992; 97:2659.
39. Caldwell J, Dang LX, Kollnian PA. J. Am. Chem. Soc. 1990; 112:9144.

40. Vorobyov IV, Anisimov VM, Alexander D, MacKerell J. J. Phys. Chem. B. 2005; 109:18988. [PubMed: 16853445]
41. Ren P, Ponder JW. J. Comp. Chem. 2002; 23:1497. [PubMed: 12395419]
42. Patel S, C. L. B. J. Comp. Chem. 2004; 25:1504. [PubMed: 15224394]
43. Patel S, C. L. B. Molecular Simulation. 2006; 32:231.
44. Kaminski GA, Stern HA, Berne BJ, Friesner RA. J. Phys. Chem. A. 2004; 108:621.
45. Kaminski GA, Stern HA, Berne BJ, Friesner RA, Cao YX, Murphy RB, Zhou R, Halgren TA. J. Comp. Chem. 2002; 23:1515. [PubMed: 12395421]
46. Banks JL, Kaminski GA, Zhou R, Mainz DT, Berne BJ, Friesner RA. J. Phys. Chem. B. 1999; 110:741.
47. Stern H, Kaminski GA, Banks JL, Zhou R, Berne BJ, Friesner RA. J. Phys. Chem. B. 1999; 103:4730.
48. Gresh N. J. Comp. Chem. 1995; 16:856.
49. Gresh N, Garmer DR. J. Comp. Chem. 1996; 17:1481.
50. Ledecq M, Lebon F, Durant F, Giessner-Prettre C, Marquez A, Gresh N. J. Phys. Chem. B. 2003; 107:10640.
51. Stern H, Rittner F, Berne BJ, Friesner R. J. Chem. Phys. 2001; 115:2237.
52. Dang LX, Chang TM. J. Chem. Phys. 1997; 106:8149.
53. Ren R, Ponder JW. J. Phys. Chem. B. 2003; 107:5933.
54. Gao J, Habibollazadeh D, Shao L. J. Phys. Chem. 1995; 99:16460.
55. Lamoureux G, A. D. M. Roux B. J. Chem. Phys. 2003; 119:5185.
56. Lamoureux G, Roux B. J. Chem. Phys. 2003; 119:3025.
57. Anisimov VM, Lamoureux G, Vorobyov IV, Huang N, Roux B, Alexander D, MacKerell J. J. Chem. Thoery Comput. 2005; 1:153.
58. Vorobyov IV, Anisimov VM, Greene S, Moser RMVA, Pastor RW, Alexander D, MacKerell J. J. Chem. Thoery Comput. 2007; 3:1120.
59. Rick SW, Stuart SJ, Berne BJ. J. Chem. Phys. 1994; 101:6141.
60. Patel S, C. L. B. J. Chem. Phys. 2005; 123:164502. [PubMed: 16268707]
61. Rick SW, Stuart SJ, Bader JS, Berne BJ. J. Mol. Liq. 1995; 65/66:31.
62. Rick SW. J. Chem. Phys. 2001; 114:2276.
63. Rappe AK, Goddard WA III. J. Phys. Chem. 1991; 95:3358.
64. Patel S, C. L. B. J. Comp. Chem. 2004; 25:1. [PubMed: 14634989]
65. Mortier WJ, Ghosh SK, Shankar S. J. Am. Chem. Soc. 1986; 108:4315.
66. Mortier WJ, Genechten KV, Gasteiger J. J. Am. Chem. Soc. 1985; 107:829.
67. Olana LR, Rick SW. J. Comp. Chem. 2005; 26:699. [PubMed: 15761861]
68. Kuo IW, Mundy CJ. Science. 2004; 303:658. [PubMed: 14752157]
69. Wiek C, Kuo IW, Mundy C, Dang LX. J. Chem. Thoery Comput. 2007; 3:2002.
70. Vassilev R, Hartnig C, Köper MTM, Frechard F, van Stanten RA. J. Chem. Phys. 2001; 115:9815.
71. Wiek CD, Dang LX. J. Phys. Chem. B. 2006; 110:6824. [PubMed: 16570991]
72. Wiek CD, Dang LX, Jungwirth P. J. Chem. Phys. 2006; 125:024706.
73. Jungwirth R, Tobias DJ. J. Phys. Chem. B. 2002; 106:6361.
74. Jungwirth R, Winter B. Ann. Rev. of Phys. Chem. 2008; 59:343. [PubMed: 18031215]
75. Liu R, Härder E, Berne BJ. J. Phys. Chem. B. 2005; 109:2949. [PubMed: 16851308]
76. Matsumoto M, Kataoka Y. J. Chem. Phys. 1988; 88:3233.
77. Dang LX, Chang T-M. J. Phys. Chem. B. 2002; 106:235.
78. Kuo IW, Mundy CJ, Eggiman BL, McGrath MJ, Siepmann JL, Chen B, Vieceli J, Tobias DJ. J. Phys. Chem. B. 2006; 110:3738. [PubMed: 16494432]
79. Archontis G, Leontidis E, Andreou GJ. Phys. Chem. B. 2005; 109:17957.
80. Matsumoto M, Kataoka Y. J. Chem. Phys. 1989; 90:2390.
81. Wilson MA, Pohorille A, Pratt LR. J. Chem. Phys. 1988; 88:3281. [PubMed: 11542143]

82. Sokhan VP, Tildesley D. J. Mol. Phys. 1997; 92:625.
83. Liu P, Harder E, Berne BJ. J. Phys. Chem. B. 2004; 108:6595.
84. Paul S, Chandra A. Chem. Phys. Lett. 2003; 373:87.
85. Wick CD, Dang LX. J. Phys. Chem. B. 2005; 109:15574. [PubMed: 16852975]
86. Xu H, Berne BJ. J. Phys. Chem. B. 2002; 106:2054.
87. Motakabbir KA, Berkowitz ML. Chem. Phys. Lett. 1991; 176:61.
88. Silvestrelli PL, Parrinello M. Phys. Rev. Lett. 1999; 82:3308.
89. Clough SA, Beers Y, Klein GP, Rothman LS. J. Chem. Phys. 1973; 59:2254.
90. Badyal YS, Saboungi ML, Price DL, Shastri SD, Haeffner DR, Soper AK. J. Chem. Phys. 2000; 112:9206.
91. Warren GL, Patel S. J. Chem. Phys. 2007; 064509:127.
92. Warren GL, Patel S. J. Phys. Chem. C. 2008 ASAP Article, DOI 10.1021/jp712136e S1932-7447(71)02136-8.
93. Brooks BR, Bruccoleri RE, Olafson BD, Stages DJ, Swaniinathan S, Karplus MJ. J. Comp. Chem. 1983; 4:187.
94. Ryckaert JP, Ciccotti G, Berendsen HJC. J. Comp. Phys. 1977; 23:327.
95. Darden T, York D, Pedersen L. J. Chem. Phys. 1993; 98:10089.
96. Essniann U, Perera L, Berkowitz ML, Darden T, Pedersen LG. J. Chem. Phys. 1995; 103:8577.
97. Parfenyuk VI. Colloid J. 2002; 64:588.
98. Paluch M. Adv. Colloid Interface Sci. 2000; 84:27. [PubMed: 10696451]
99. Wilson MA, Pohorille A, Pratt LR. J. Chem. Phys. 1989; 90:5211. [PubMed: 11542468]
100. Kastenholz MA, Hunenberger PH. J. Chem. Phys. 2006; 124:224501. [PubMed: 16784292]
101. Pandit SA, Bostick D, Berkowitz ML. Biophys. J. 2003; 85:3120. [PubMed: 14581212]
102. Landau, LD.; Lifshitz, EM. Electrodynamics of Continuous Media. Perganion: 1960.
103. Pratt LR. J. Phys. Chem. 1992; 96:25.
104. Zakharov VV, Brodskaya EN, Laaksonen A. J. Chem. Phys. 1997; 107:1997.
105. Torrie GM, Patey GN. J. Phys. Chem. 1993; 97:12909.
106. Randies JE. B. Phys. Chem. Liq. 1977; 7:107.
107. Jackson, JD. Classical Electrodynamics. 3rd ed.. Wiley; New York: 1998. p. 641
108. Jaqaman K, Tuncay K, Ortoleva PJ. J. Chem. Phys. 2004; 120:926. [PubMed: 15267929]
109. Heinz TN, Hunenberger PH. J. Chem. Phys. 2005; 123:034107.
110. Herce DH, Perera L, Darden TA, Sagui C. J. Chem. Phys. 2005; 122:024513. [PubMed: 15638604]

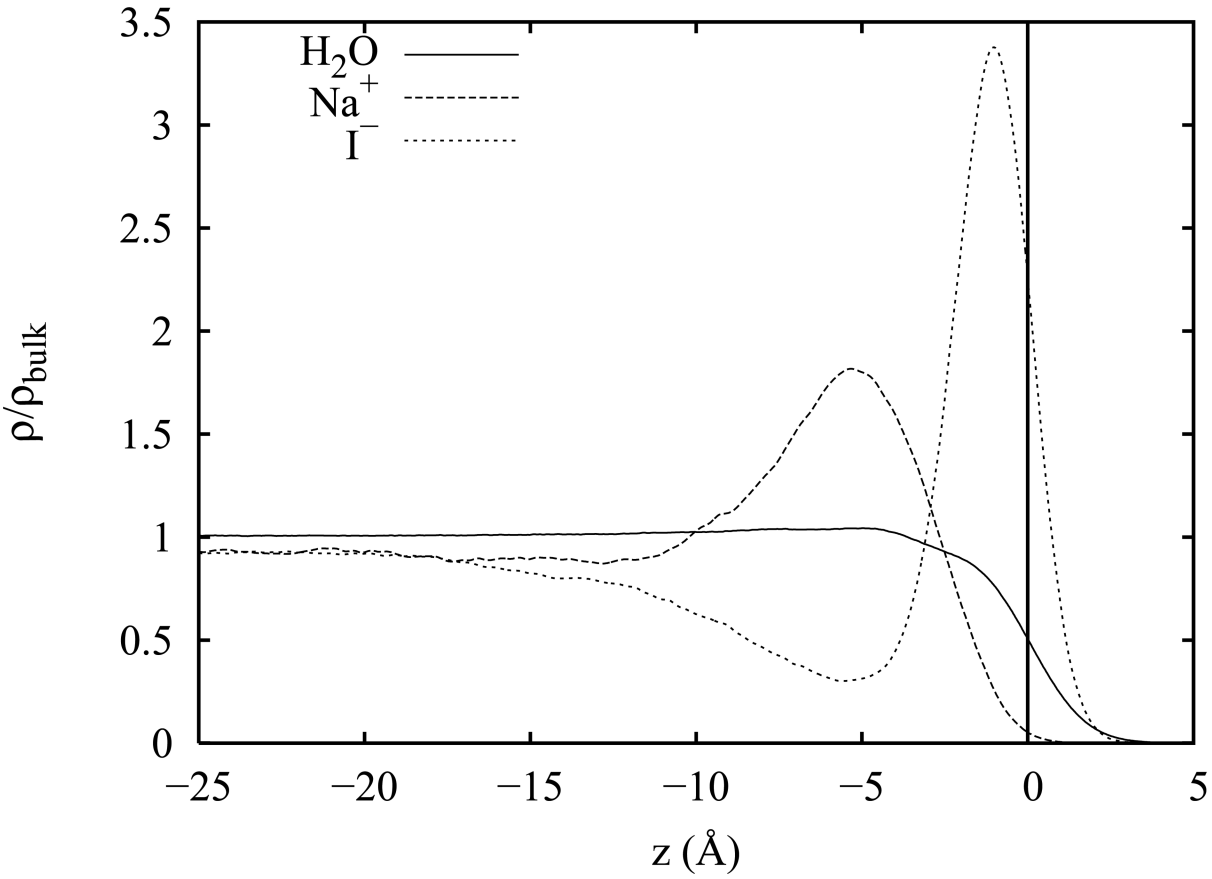


**Figure 1.**
A representative salt density profile for NaI. Densities are normalized relative to the corresponding densities obtained from periodic bulk simulations.

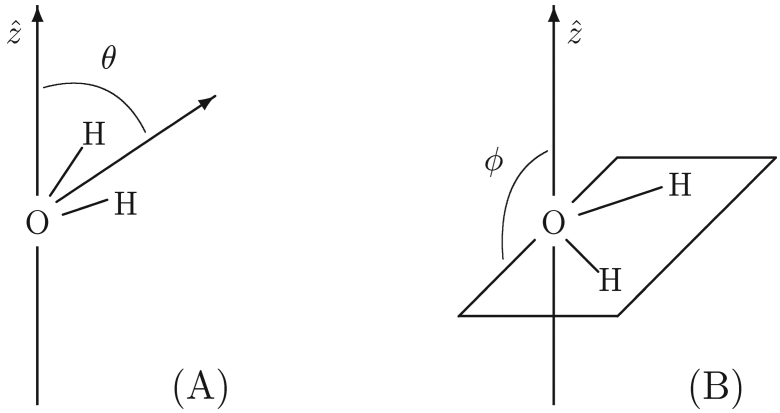


**Figure 2.**
Angles $\theta$ (panel A) and $\varphi$ (panel B) used in describing the orientation of water molecules relative to the surface normal ($\hat{z}$ direction).

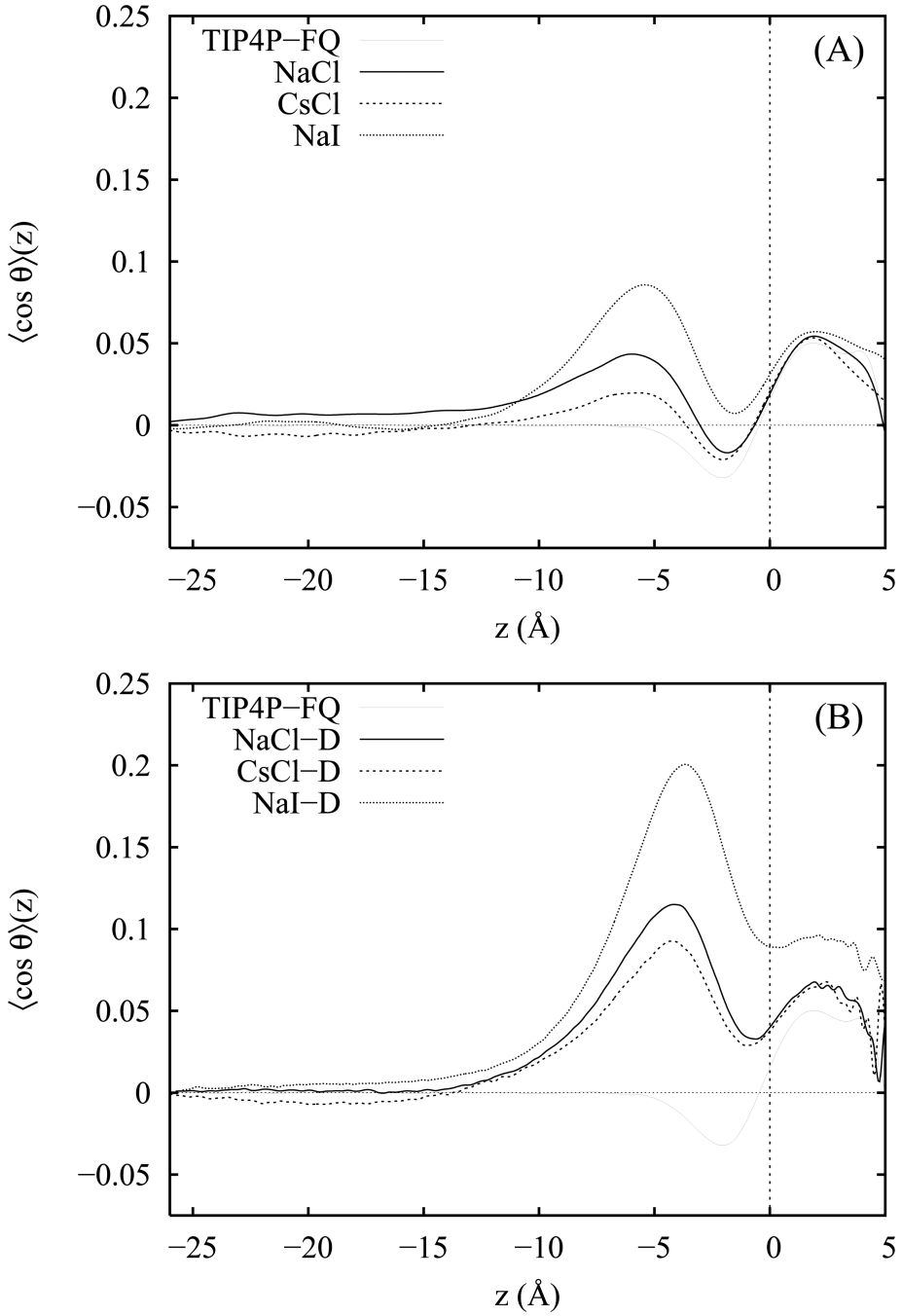


**Figure 3.**

The orientational distribution function $\langle \cos \theta \rangle (z)$ as a function of distance $z$ from the Gibbs dividing surface ($z = 0$) plotted for neat water and 1 M solutions of NaCl, CsCl and NaI. Results for the non-polarizable and Drude-polarizable ion models are plotted in panels A and B, respectively.

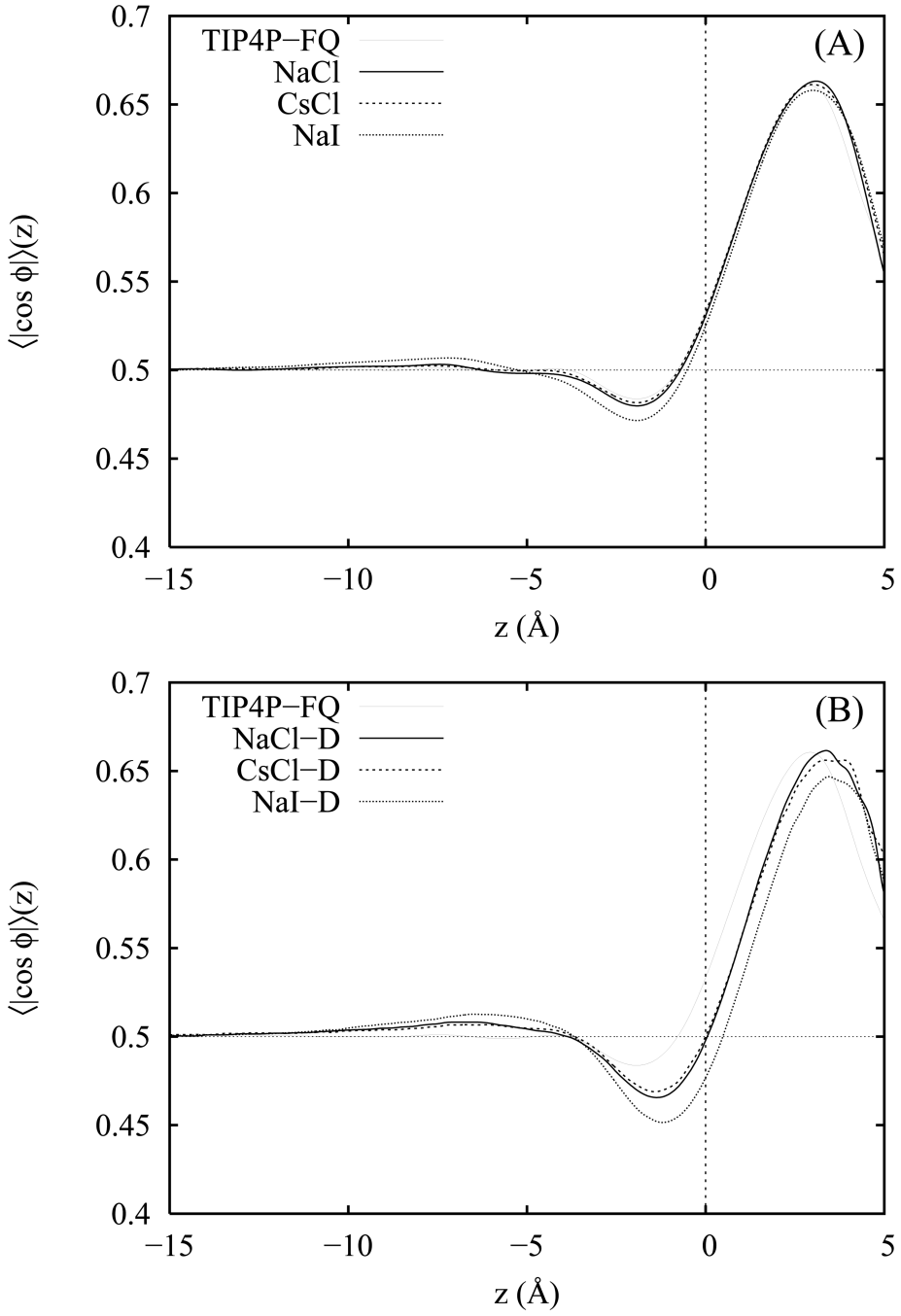


**Figure 4.**

The orientational distribution function $\langle|\cos\varphi|\rangle(z)$ as a function of the distance $z$ from the Gibbs dividing surface ($z = 0$) plotted for neat water and 1 M solutions of NaCl, CsCl and NaI. Results for the non-polarizable and Drude-polarizable ion models are plotted in panels A and B, respectively.

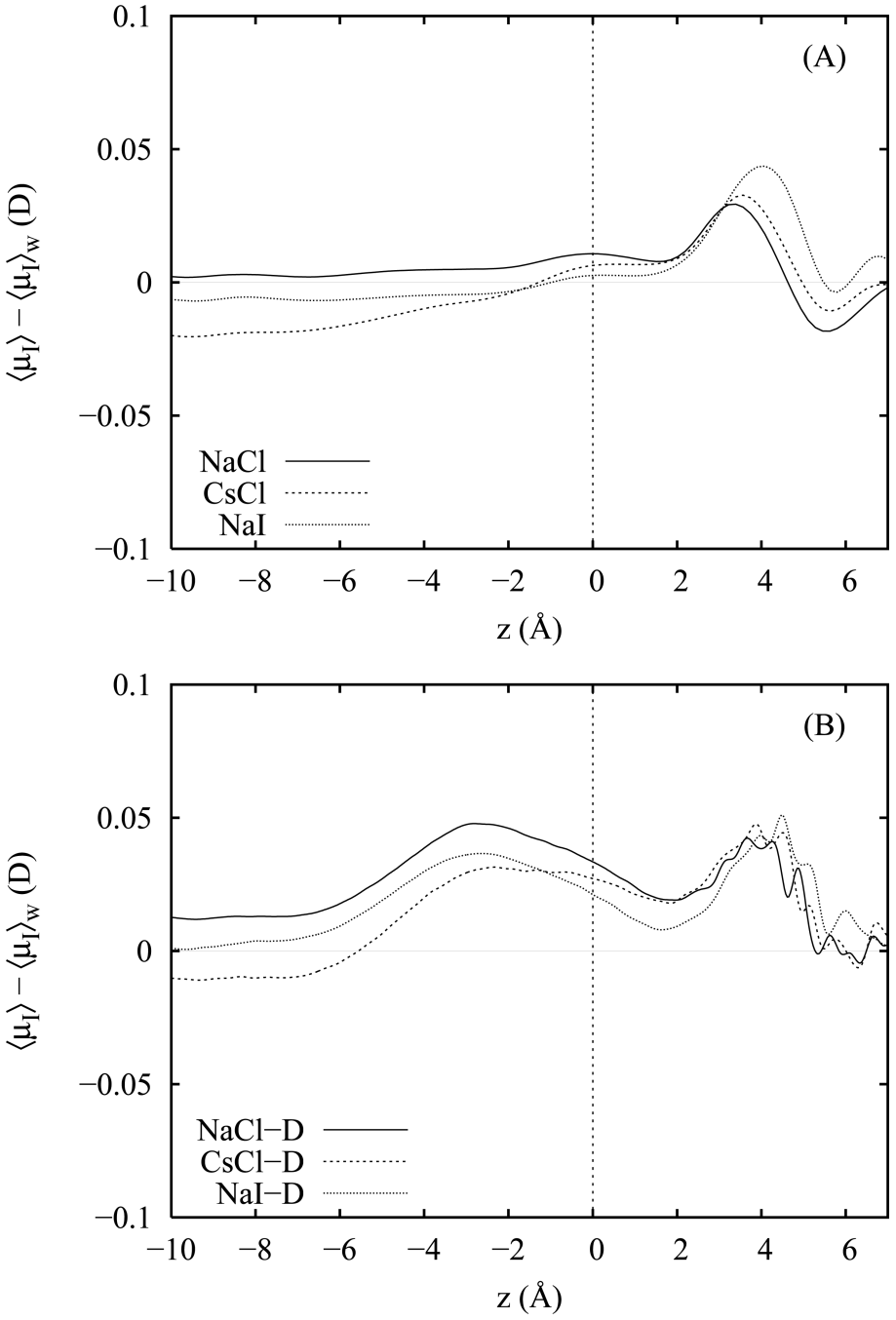


**Figure 5.**

Average magnitude of the total water induced dipole moment less the total induced dipole moment of neat TIP4P-FQ water as a function of the distance *z* from the Gibbs dividing surface (*z* = 0). Moments are plotted for 1 M solutions of NaCl, CsCl and NaI employing non-polarizable (panel A) and polarizable (panel B) ion models.

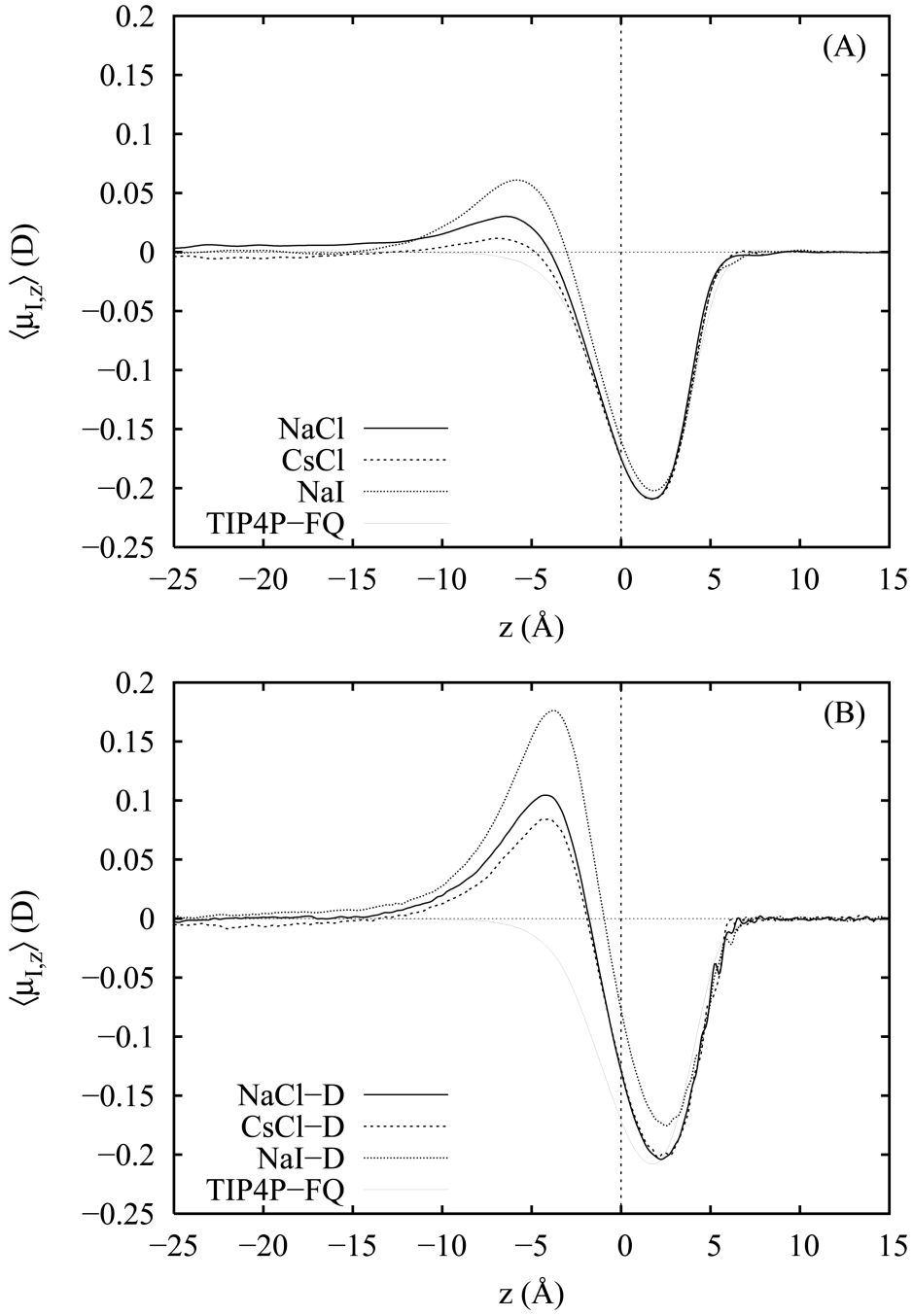


**Figure 6.**

Average magnitude of the *z* component of the water induced dipole moment as a function of the distance *z* from the Gibbs dividing surface (*z* = 0). Moments are plotted for 1 M solutions of NaCl, CsCl and NaI employing non-polarizable (panel A) and polarizable (panel B) ion models.

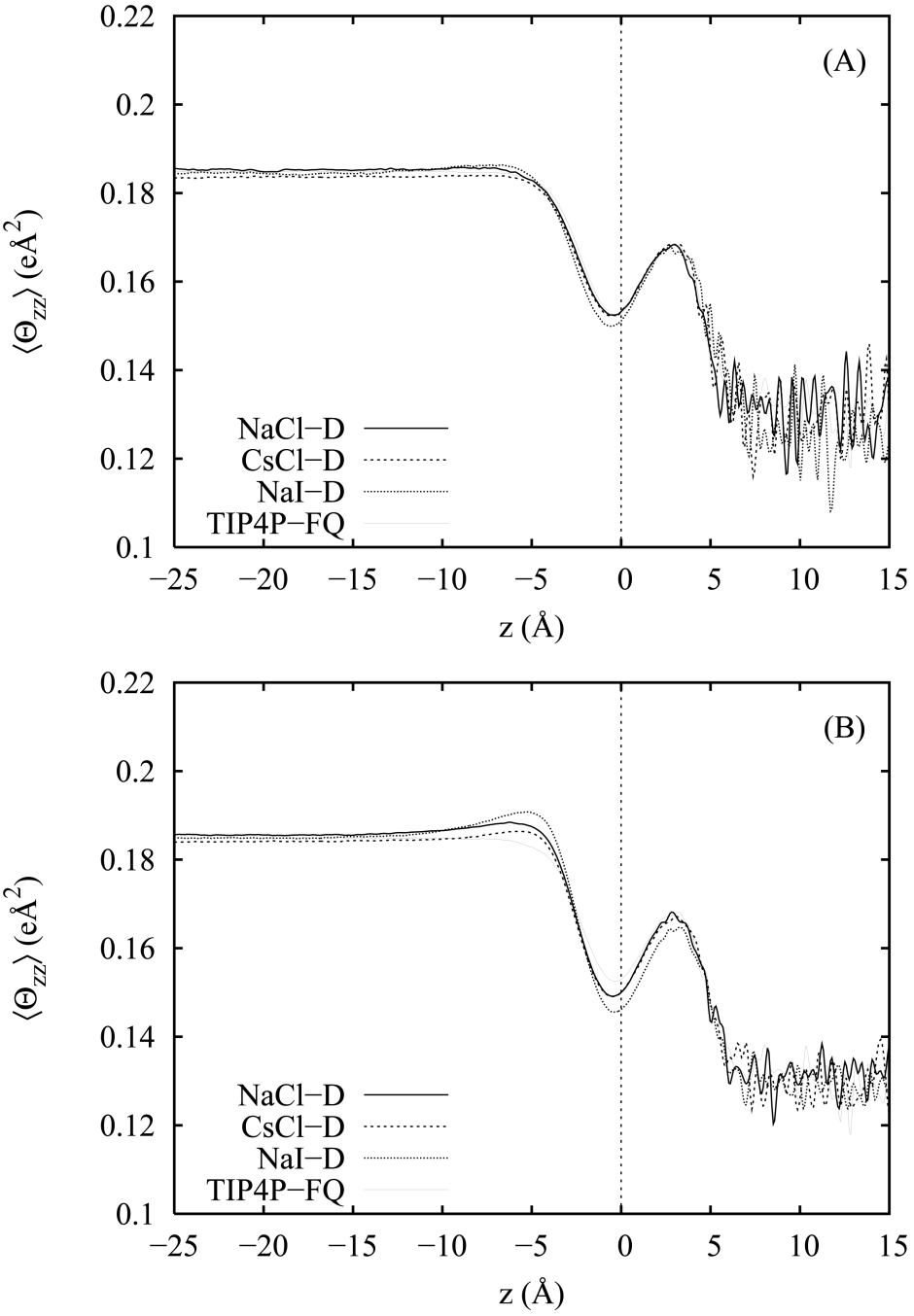


**Figure 7.**

Average magnitude of the *zz* component of the water induced quadrupole moment as a function of the distance *z* from the Gibbs dividing surface (*z* = 0). Moments are plotted for 1 M solutions of NaCl, CsCl and NaI employing non-polarizable (panel A) and polarizable (panel B) ion models.

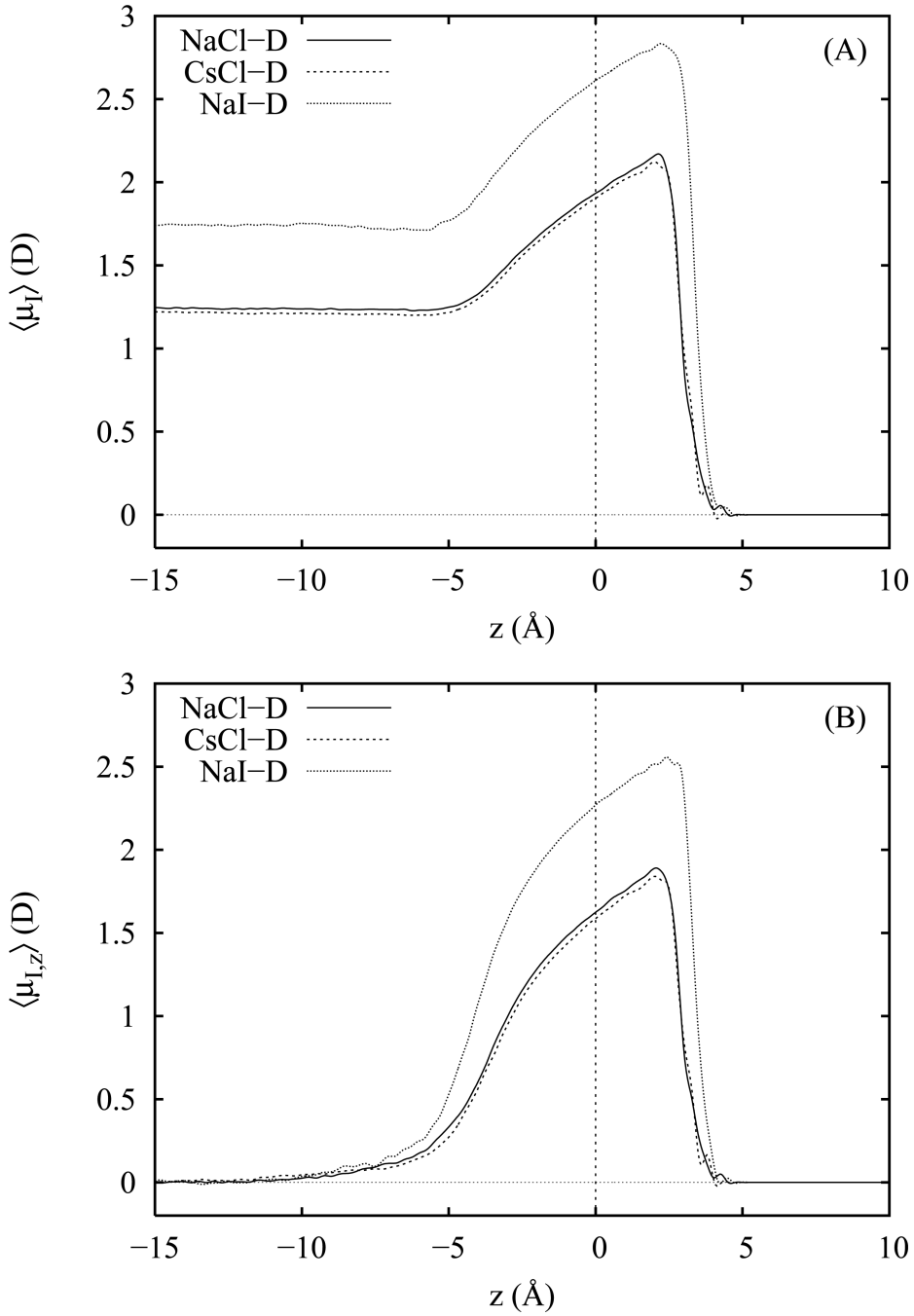


**Figure 8.**

Average magnitudes of the total (panel A) and *z* projection of the anion induced dipole moments as a function of the distance *z* from the Gibbs dividing surface (*z* = 0). Moments are plotted for 1 M solutions of NaCl, CsCl and NaI employing Drude-polarizable ion models.

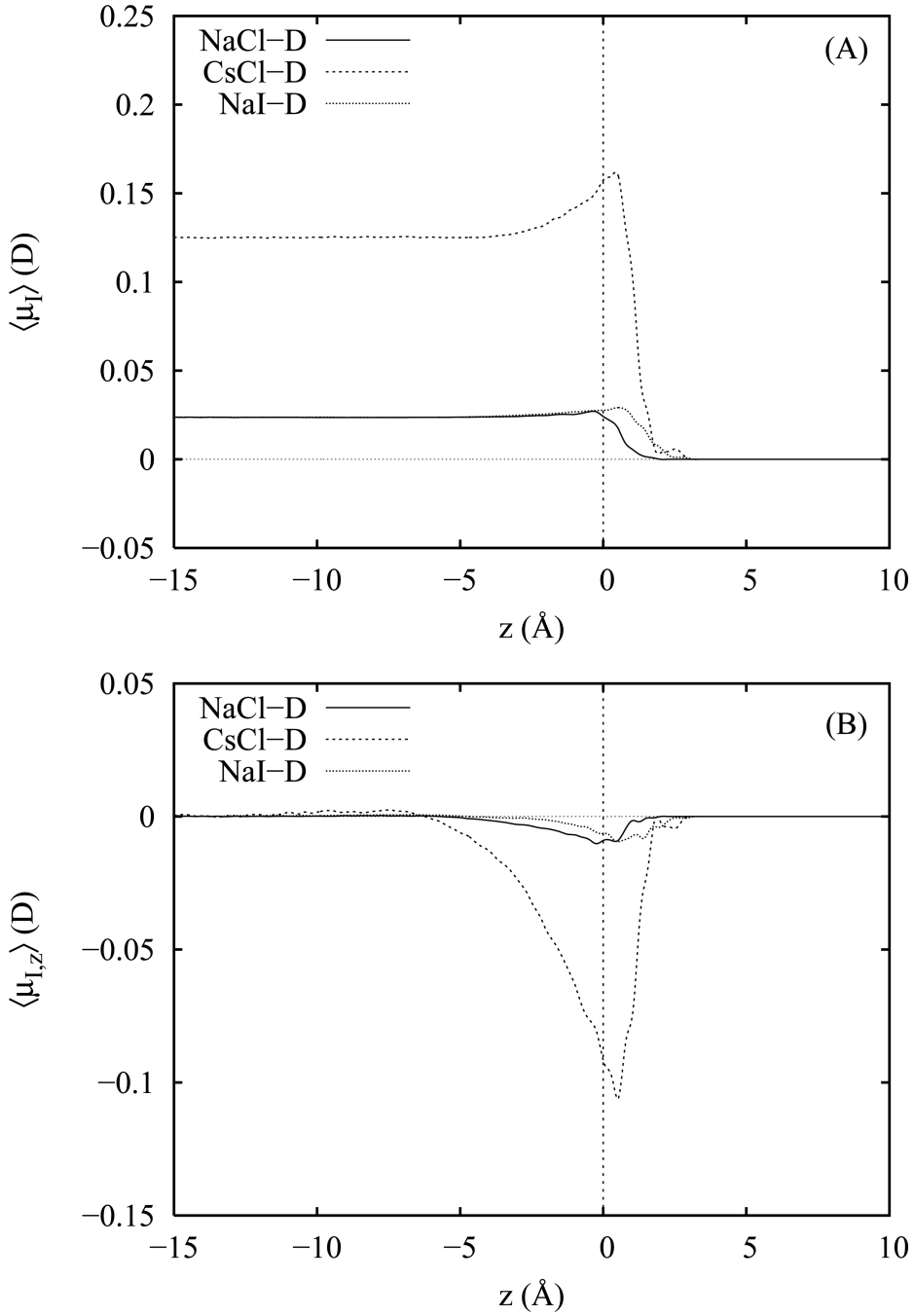


**Figure 9.**

Average magnitudes of the total (panel A) and *z* projection of the cation induced dipole moments as a function of the distance *z* from the Gibbs dividing surface (*z* = 0). Moments are plotted for 1 M solutions of NaCl, CsCl and NaI employing Drude-polarizable ion models.

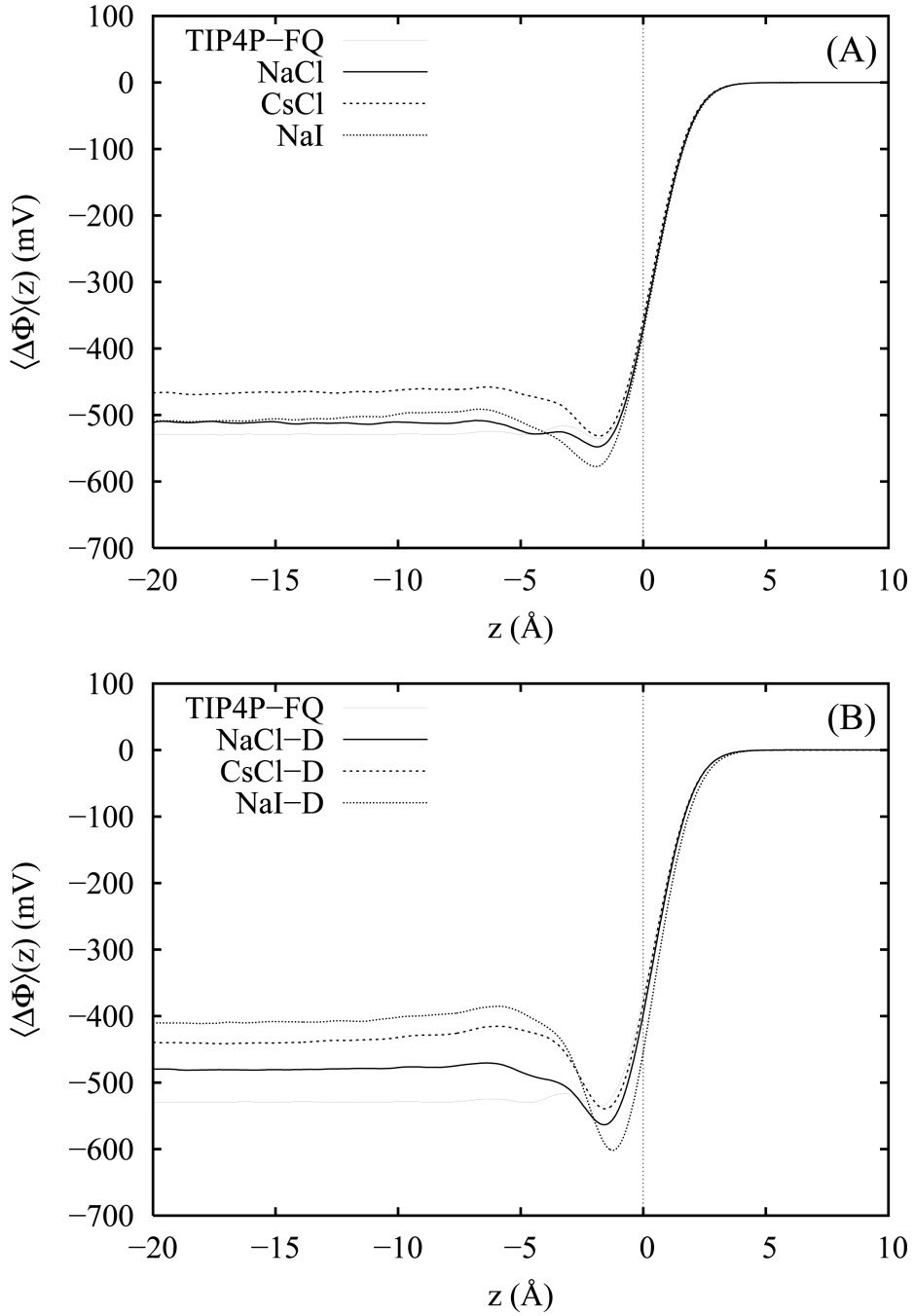


**Figure 10.**

The total interfacial potential **ΔΦ** (mV) of equation 1 plotted as a function of the distance *z* from the Gibbs dividing surface (*z* = 0) for neat water and 1 M solutions of NaCl, CsCl and NaI modeled with non-polarizable (panel A) and Drude-polarizable (panel B) ion potentials.

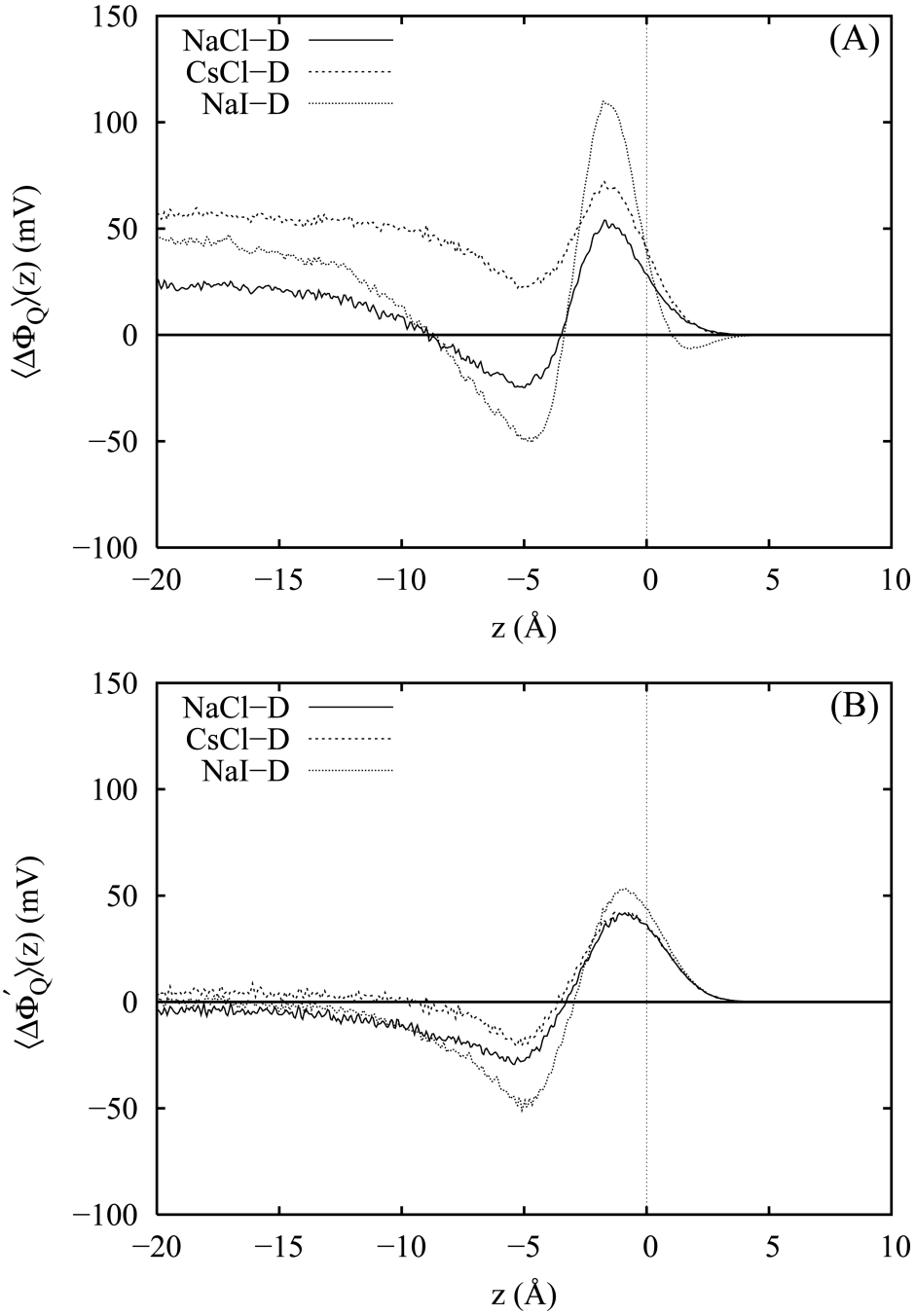


**Figure 11.**

Panel A: The quadrupole potential contributions of the interfacial potential for the three Drude-polarizable salt models less the corresponding quadrupole contributions of neat TIP4P-FQ water. Panel B: The modified quadrupole potential function $\Delta\Phi'_Q$ for the Drude-polarizable salt models obtained by adjusting the quadrupole potentials for the relative changes in the water density profiles between the salt solutions and neat water.

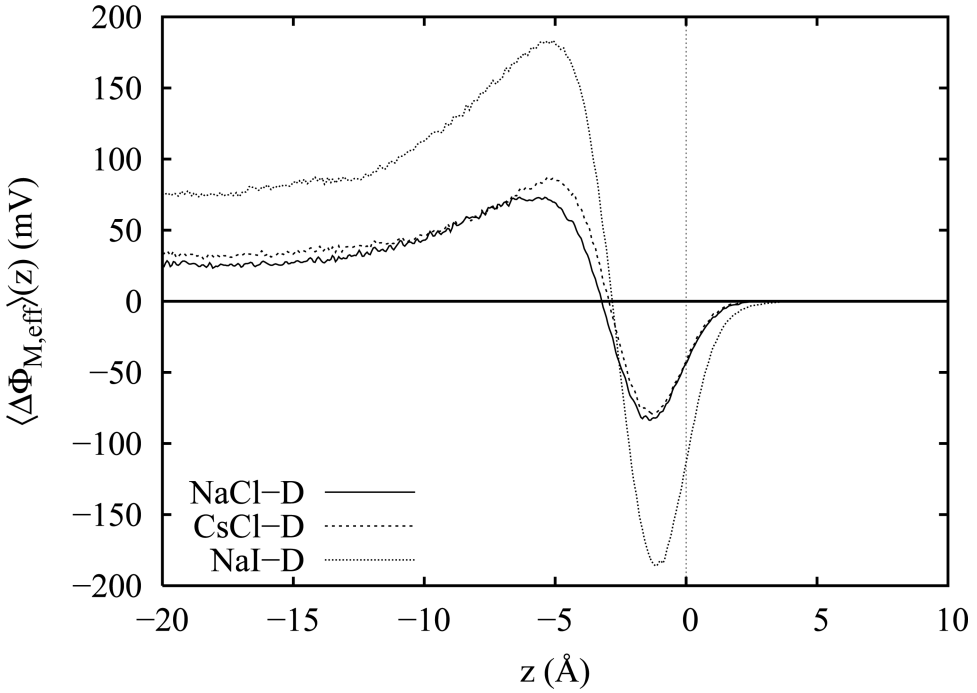


**Figure 12.**

The “effective” dipole potential contributions to the interfacial potential for the three Drude-polarizable salt models less the corresponding total dipole potential of neat TIP4P-FQ water.

**TABLE I**

A decomposition of the total interfacial potential into components arising from the water total dipole moment ($\Delta\Phi_M(H_2O)$), the water quadrupole moment ($\Delta\Phi_Q(H_2O)$), the ion monopoles ($\Delta\Phi_q(M^+A^-)$) and the ion induced dipoles ($\Delta\Phi_M(M^+A^-)$). The total interfacial potential derived from equation 1) is provided for comparison. All potentials are in units of mV

| Salt Model | $\Delta\Phi_M(H_2O)$ | $\Delta\Phi_Q(H_2O)$ | $\Delta\Phi_q(M^+A^-)$ | $\Delta\Phi_M(M^+A^-)$ | $\Delta\Phi_{total}$ | $\Delta\Phi$ (eq 1) | $\Delta\Delta\Phi$ | $\Delta\Delta\Phi_{pol}$ |
|---|---|---|---|---|---|---|---|---|
| Neat water | 594 | –1124 | – | – | –530 | –529 ± 2 | – | – |
| NaCl | –704 | –1099 | 1293 | – | –510 | –511 ± 4 | 18 | – |
| NaCl-D | –2169 | –1101 | 2972 | –181 | –479 | –481 ± 4 | 48 | 30 |
| CsCl | 353 | –1052 | 228 | – | –471 | –467 ± 4 | 62 | – |
| CsCl-D | –1440 | –1066 | 2231 | –168 | –444 | –440 ± 5 | 89 | 27 |
| NaI | –1269 | –1063 | 1829 | – | –503 | –508 ± 5 | 21 | – |
| NaI-D | –4047 | –1079 | 5186 | –471 | –411 | –410 ± 8 | 119 | 98 |